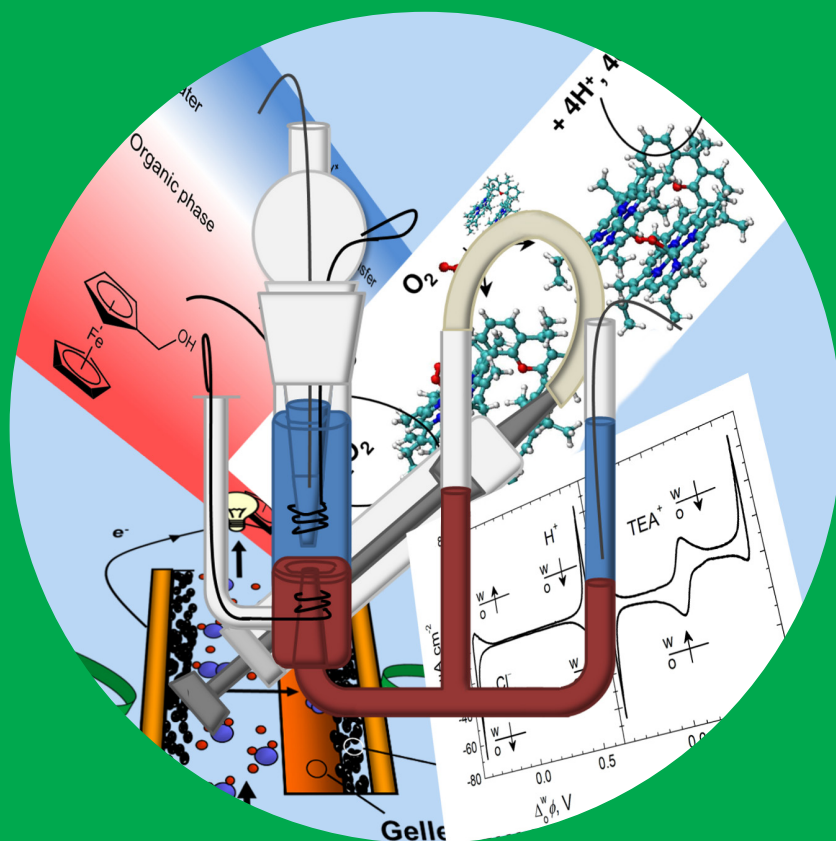


Proton Transfer Controlled Reactions at Liquid-Liquid Interfaces

Pekka Peljo



Proton Transfer Controlled Reactions at Liquid-Liquid Interfaces

Pekka Peljo

Doctoral dissertation for the degree of Doctor of Science in Technology to be presented with due permission of the School of Chemical Technology for public examination and debate in Auditorium KE2 (Komppa Auditorium) at the Aalto University School of Chemical Technology (Espoo, Finland) on the 5th of April, 2013, at 12 noon.

Aalto University
School of Chemical Technology
Department of Chemistry
Research Group of Physical Chemistry and Electrochemistry

Supervising professor

Professor Kyösti Kontturi

Thesis advisor

Dr. Lasse Murtomäki

Preliminary examiners

Professor Robert Dryfe, University of Manchester, United Kingdom

Professor Bin Su, Zhejiang University, China

Opponent

Professor Zdeněk Samec, J. Heyrovský Institute of Physical
Chemistry of ASCR, Czech Republic

Aalto University publication series

DOCTORAL DISSERTATIONS 39/2013

© Pekka Peljo

ISBN 978-952-60-5050-8 (printed)

ISBN 978-952-60-5049-2 (pdf)

ISSN-L 1799-4934

ISSN 1799-4934 (printed)

ISSN 1799-4942 (pdf)

<http://urn.fi/URN:ISBN:978-952-60-5049-2>

Unigrafia Oy

Helsinki 2013

Finland



Author

Pekka Peljo

Name of the doctoral dissertation

Proton Transfer Controlled Reactions at Liquid-Liquid Interfaces

Publisher School of Chemical Technology

Unit Department of Chemistry

Series Aalto University publication series DOCTORAL DISSERTATIONS 39/2013

Field of research Physical Chemistry

Manuscript submitted 10 December 2012

Date of the defence 5 April 2013

Permission to publish granted (date) 12 February 2013

Language English

Monograph

Article dissertation (summary + original articles)

Abstract

Electrochemistry at liquid-liquid interfaces has been a versatile area of contemporary electrochemistry for almost 40 years, with research mainly focusing on the aqueous-organic solution interface. The Galvani potential difference across such an interface, controlling the distribution of ions between the phases, can be generated either chemically or with an external voltage source. An aqueous-organic solvent interface shares similarities with the cell membrane, where several important biological reactions such as photosynthesis or cell respiration take place. Hence electrochemistry at liquid-liquid interfaces is an excellent means to study biomimetic oxygen reduction. In this reaction, proton transfer across the interface controlled by the Galvani potential difference is coupled with electron transfer. Therefore oxygen reduction in the oil phase mediated by an electron donor occurs only at potentials where proton transfer becomes feasible.

In this thesis oxygen and hydrogen peroxide reduction by 1,2-diferrocenylethane was investigated. The results show that the reduction of hydrogen peroxide is faster than oxygen reduction, but both reactions were slow due to the low thermodynamic driving force. The reaction rate can be increased by the addition of molecular catalysts, and electrochemistry at liquid-liquid interfaces provides an excellent means to compare the activity and selectivity of the catalysts. Cofacial cobalt porphyrins, biomimetic analogues of the active centre of cytochrome *c* oxidase responsible of oxygen reduction in nature, were investigated. Surprisingly, significant amounts of hydrogen peroxide were produced, contradicting previous results. The reaction was shown to proceed to hydrogen peroxide when oxygen was bound to the exo side (dock-on) of the catalyst, while four-electron reduction took place with oxygen bound to the endo side (dock-in) of the molecule.

A proof of concept of a novel type of a fuel cell utilising the liquid-liquid interface is presented. In this fuel cell hydrogen is oxidized on the anode as in a conventional fuel cell, but oxygen reduction takes place at the liquid-liquid interface. The redox mediator in the oil phase is regenerated at the cathode, completing the electric circuit.

Proton transfer across the interface was also utilised for performing acid catalysed S_N1 substitutions on ferrocene methanol. This is a novel method to perform synthesis of organic chemicals, as the presence of protons is controlled by the applied Galvani potential difference. *In situ* biphasic electrospray ionization mass spectroscopy was demonstrated to be a very efficient way to follow this kind of reactions.

Keywords liquid-liquid interfaces, electrochemistry, electrocatalysis, oxygen reduction, proton transfer catalysis, fuel cells, proton-coupled electron transfer

ISBN (printed) 978-952-60-5050-8

ISBN (pdf) 978-952-60-5049-2

ISSN-L 1799-4934

ISSN (printed) 1799-4934

ISSN (pdf) 1799-4942

Location of publisher Espoo

Location of printing Helsinki

Year 2013

Pages 158

urn <http://urn.fi/URN:ISBN:978-952-60-5049-2>

Tekijä

Pekka Peljo

Väitöskirjan nimi

Protonin siirron kontrolloimat reaktiot neste-nesterajapinnalla

Julkaisija Kemian tekniikan korkeakoulu**Yksikkö** Kemian laitos**Sarja** Aalto University publication series DOCTORAL DISSERTATIONS 39/2013**Tutkimusala** Fysikaalinen kemia**Käsikirjoituksen pvm** 10.12.2012**Väitöspäivä** 05.04.2013**Julkaisuluvan myöntämispäivä** 12.02.2013**Kieli** Englanti **Monografia** **Yhdistelmäväitöskirja (yhteenveto-osa + erillisartikkelit)****Tiivistelmä**

Neste-nesterajapintojen sähkökemian on ollut yksi modernin sähkökemian osa-alueista jo lähes 40 vuoden ajan. Tutkimus on pääasiassa keskittynyt varauksensiirtoon veden ja orgaanisen liuoksen välisellä rajapinnalla. Faasien välinen galvaanipotentiaaliero, joka kontrolloi ionien jakautumista niiden välillä, saadaan aikaan joko kemiallisesti tai ulkoisella jännitelähteellä. Monet luonnossa tapahtuvat tärkeät reaktiot, kuten fotosynteesi tai soluhengitys, tapahtuvat solukalvossa, joka muistuttaa veden ja orgaanisen liottimen rajapintaa. Siksi neste-nesterajapintojen sähkökemian on erinomainen tapa tutkia bio- mimeettistä hapen pelkistystä. Hapen pelkistyksessä galvaanipotentiaalieron kontrolloima protonin siirto kytkeytyy yhteen elektroninsiirron kanssa. Happi pelkistyy orgaanisessa faasissa vain, kun faasien välinen galvaanipotentiaaliero on niin suuri, että protoni voi siirtyä rajapinnan yli.

Tässä työssä tutkittiin hapen ja vetyperoksidin pelkistämistä 1,2-diferrosenyyliaaniilla. Tulokset osoittivat, että vetyperoksidin pelkistys on hapen pelkistystä nopeampaa, mutta molemmat reaktiot ovat hitaita heikon termodynaamisen ajavan voiman takia. Reaktiota voidaan nopeuttaa käyttämällä molekulaarisia katalyyttejä, ja neste-nesterajapintojen sähkökemian on erinomainen tapa vertailla eri katalyyttien selektiivisyyttä ja aktiivisuutta. Työssä tutkittiin sytokromi-*c*-oksidaasin aktiivista keskusta muistuttavia biskobolttiporfyyriinejä, sillä sytokromi-*c*-oksidaasi on ainoa luonnollinen happea pelkistävä entsyymi. Yllätykseksemme nämä katalyytit tuottivat merkittäviä määriä vetyperoksidia edellisten tulosten vastaisesti. Tulokset osoittivat, että vetyperoksidia syntyy hapen sitoutuessa katalyytin ulkopuolelle, ja pelkistys vedeksi tapahtuu hapen sitoutuessa bisporfyyriinin sisälle, joten hapen pelkistys biskobolttiporfyyriineillä tapahtuu ”dock-on/dock-in” mekanismin mukaisesti. Hapen pelkistystä neste-nesterajapinnalla voidaan myös käyttää uudenlaisessa polttokennossa. Kennossa vety hapettuu anodilla kuten tyypillisessäkin polttokennossa, mutta happi pelkistyy neste-nesterajapinnalla. Redoxmediaattori regeneroidaan katodilla, mikä sulkee sähköisen virtapiirin.

Protonin siirtoa neste-nesterajapinnan yli voidaan käyttää myös katalysoimaan ferroseenimetanolin S_N1 -substituutiota. Tässä uudenlaisessa orgaanisten kemikaalien synteesimenetelmässä reaktio voidaan aloittaa tai lopettaa kontrolloimalla galvaanipotentiaalieron avulla katalyytin eli protonin konsentraatiota orgaanisessa faasissa. Kaksifaasinen elektronisuihuionisaatiomassaspektroskopia osoittautui erinomaiseksi tekniikaksi tämänkaltaisten reaktioiden seurantaan ja reaktiotuotteiden analysointiin.

Avainsanat neste-nesterajapinnat, sähkökemian, elektrokatalyyysi, hapen pelkistys, protoninsiirtokatalyyysi, polttokennot, protoninsiirtoon kytketty elektroninsiirto

ISBN (painettu) 978-952-60-5050-8**ISBN (pdf)** 978-952-60-5049-2**ISSN-L** 1799-4934**ISSN (painettu)** 1799-4934**ISSN (pdf)** 1799-4942**Julkaisupaikka** Espoo**Painopaikka** Helsinki**Vuosi** 2013**Sivumäärä** 158**urn** <http://urn.fi/URN:ISBN:978-952-60-5049-2>

Preface

The work presented in this thesis was carried out mainly at the Research Group of Physical Chemistry and Electrochemistry, Department of Chemistry, Aalto University between December 2009 and December 2012. The work for Publication I and partly for III was performed at Laboratoire d'Electrochimie Physique et Analytique, Ecole Polytechnique Fédérale de Lausanne, Switzerland, between September 2011 and February 2012. I am grateful for the financial support for this project from the Academy of Finland and for my visit to Switzerland from the Magnus Ehrnrooth foundation.

Firstly, I would like to express my gratitude for my supervisor Prof. Kyösti Kontturi for giving me the opportunity and arranging the funding to study this interesting topic for my post graduate studies. I would also like to thank my thesis advisor Dr. Lasse Murtomäki for all the helpful discussions and suggestions during this work, as well as Dr. Tanja Kallio for her help and comments regarding especially the fuel cells but also other parts of this work. Additionally, I am also grateful for Dr. Christoffer Johans for all the discussions concerning the electrochemistry at liquid-liquid interfaces.

Secondly, I am grateful to Prof. Hubert Girault for the opportunity to spend six months at LEPA, as well as for all the helpful discussions, constant enthusiasm and exiting new ideas during this work. Related to my time in Lausanne, I want to thank my co-authors Mr. Haiqiang Deng, Ms. Peiyu Ge and Dr. Fernando Cortés-Salazar for the help, input and company during this work and Mr. Liang Qiao for sparing some time to try something new with his ESI-MS set-up. I also want to thank Mrs. Astrid Olaya for her input and suggestions, and for her patience with the SSHG set-up. Additionally, I wish to thank all the people at LEPA, especially Dr. Micheal Scanlon and Dr. Kathryn Toghil, for the good time in Lausanne. Also not forgetting the Chinese group, it was very nice to go hiking or skiing on the Swiss Alps.

I am also grateful to my other co-authors Dr. Hai-Jun Xu, Dr. Michel Meyer, Dr. Claude P. Gros and Prof. Jean-Michel Barbe from Institut de Chimie Moléculaire de l'Université de Bourgogne, Dijon, for fruitful collaboration and for all the help, suggestions and feedback during the preparation of the manuscript. Prof. Kari Laasonen from Aalto University is acknowledged for coming to our rescue with his DFT calculations when experimental results were giving unexpected results.

Special thanks belong to my summer workers Ms. Taina Rauhala, Mr. Taneli Rajala and Mr Carsten Mecke for all the good work they did when I was away sailing. The valuable help from Mr. David Lloyd, Dr. Ben Wilson and Dr. Kathryn Toghil for proof-reading the thesis is gratefully acknowledged.

Many thanks belong to all the personnel and PhD students of the laboratory of Physical Chemistry and Electrochemistry. Special thanks go for all the people in the fuel cell group, Dr. Annukka Santasalo-Aarnio, Mr. Petri Kanninen and Mr. Sami Tuomi, for all the help and suggestions during this work, and I also want to thank Petri for sharing the office with me for the past years. Big thanks also for Dr. Kirsi Yliniemi, Dr. Ben Wilson, Lic. Sc. (Tech.) Nguyet Doan, Ms. Maija Huuppola, Mr. David Loyd, Ms. Elina Pohjakallio and Mr. Tuomas Vainikka. It has been a pleasure to share my lunch and coffee breaks with you and to work here with you, making my life at FyKe a pleasant experience. Whenever I had some technical or theoretical problems, you were always ready to help. Thank you also for the technical staff of the lab, especially Dr. Annu Kontturi and Mrs. Marjut Vähänikkilä.

Finally, I would like to thank all my family and friends for being there as a counterbalance to my work. I am grateful for all your help and support with my life in general. It is good to know that you are there ready to share my problems or just go sailing with me. And to Katja, thank you for making the last few years much better just by being there.

Espoo, 24.1.2013

Pekka Peljo

Contents

1 Introduction	1
2 Electrochemistry at Liquid-Liquid Interfaces.....	4
2.1 Interface between Two Immiscible Electrolyte Solutions.....	4
2.2 Structure of the Liquid-Liquid Interface	4
2.3 Thermodynamics of the ITIES	6
2.4 Charge Transfer at the Liquid-Liquid Interface	8
2.4.1 Ion Transfer at the Liquid-Liquid Interface	8
2.4.2 Facilitated Ion Transfer at the Liquid-Liquid Interface	11
2.4.3 Electron Transfer at the Liquid-Liquid Interface	12
2.4.4 Photoinduced Charge Transfer at Liquid-Liquid Interfaces	15
3 Experimental Procedures.....	16
3.1 Four-Electrode Cell Experiments	16
3.2 Two-Phase Reactions with Chemically Controlled Polarisation.....	18
3.2.1 Analysis of the H ₂ O ₂ Produced in the Two-Phase Reaction.....	19
3.3 Ultramicroelectrode Experiments.....	20
3.4 Electrospray Ionization Mass Spectrometry.....	20
3.5 Fuel Cell Experiments	21
4 Proton-coupled Electron Transfer at Liquid-Liquid Interfaces	23
4.1 Proton-coupled Electron Transfer Reactions.....	23
4.2 Oxygen Reduction at the ITIES	24
4.2.1 Oxygen and Hydrogen Peroxide Reduction by 1,2-diferrocenylethane	25
5 Electrocatalysis at the ITIES	31
5.1 Colloidal Electrocatalysis at the ITIES	31
5.2 Molecular Electrocatalysis at the ITIES.....	32

5.2.1 Biomimetic Catalysis for Oxygen Reduction with Cofacial Porphyrins.....	37
6 Proton Transfer Catalysed Reactions at Liquid-Liquid Interfaces.....	45
6.1 Cyclic Voltammetry of Ferrocene Methanol in a Four-Electrode Cell	45
6.2 Proton Transfer Catalysed S _N 1 Substitution to Ferrocene Methanol.....	48
7 Fuel Cell Utilising a Liquid-Liquid Interface	55
8 Conclusions.....	58
8.1 Recommendations for Further Work	60
References.....	61

List of Publications

This thesis consists of an overview and of the following publications, which are referred to in the text by their Roman numerals.

- I** H. Deng, P. Peljo, F. Cortés-Salazar, P. Ge, K. Kontturi and H. H. Girault, Oxygen and hydrogen peroxide reduction by 1,2-diferrocenylethane at a liquid/liquid interface, *J. Electroanal. Chem.*, **681** (2012) 16-23.
- II** P. Peljo, L. Murtomäki, T. Kallio, X.-J. Xu, M. Meyer, C. P. Gros, J. M. Barbe, H. H. Girault, K. Laasonen and K. Kontturi, Biomimetic oxygen reduction by cofacial porphyrins at a liquid-liquid interface, *J. Am. Chem. Soc.*, **134** (2012) 5974-5984.
- III** P. Peljo, L. Qiao, L. Murtomäki, C. Johans, H. H. Girault and K. Kontturi, Electrochemically Controlled Proton-Transfer-Catalyzed Reactions at Liquid-Liquid Interfaces: Nucleophilic Substitution on Ferrocene Methanol, *ChemPhysChem*, **14** (2013) 311-314.
- IV** P. Peljo, T. Rauhala, L. Murtomäki, T. Kallio and K. Kontturi, Oxygen reduction at a water-1,2-dichlorobenzene interface catalyzed by cobalt tetraphenyl porphyrine - A fuel cell approach, *Int. J. Hydrogen Energy*, **36** (2011) 10033-10043.
- V** P. Peljo and H. H. Girault, Liquid/Liquid Interfaces: Electrochemistry at, in: R. A. Meyers (Ed.), *Encyclopedia of Analytical Chemistry*, John Wiley and Sons, Inc., Chichester, 2012. <http://dx.doi.org/10.1002/9780470027318.a5306.pub2>

Author's contribution

- Publication I The author defined the research plan together with the co-authors. The experiments, interpretation of the results and writing of the manuscript were done in co-operation with the first author.
- Publication II The author defined the research plan together with the co-authors, carried out all the experimental work excluding the synthesis of the catalysts and DFT calculations. He had a major role in interpretation of the results and he wrote the manuscript.
- Publication III The author defined the research plan, carried out the electrochemical measurements and interpreted the results. ESI-MS measurements and their interpretation were performed jointly with the first and second author. The author wrote the manuscript.
- Publication IV The research plan for this manuscript was defined together with co-authors. All the electrochemical experiments and fuel cell measurements are done or supervised by the author. The author interpreted the results and wrote the manuscript.
- Publication V The author updated the review done in year 2000, under supervision of the last author.

Espoo, 4th of December 2012

Prof. Kyösti Kontturi

List of Symbols

A	area
a	activity
c	concentration
D	diffusion coefficient
E^0	standard redox potential
$[E_{O/R}^0]_{SHE}^\alpha$	standard redox potential of O/R in phase α vs. aqueous SHE
e	elemental charge
F	Faraday's constant
$\Delta G_{tr,i}^{w \rightarrow o}$	free energy of transfer of ion i from aqueous to oil phase
ΔH	change of enthalpy
i	current
j	current density
K_a	equilibrium constant
N_a	Avogadro's constant
m	mass
n	number of transferred electrons; molar amount
P	partition coefficient
R	molar gas constant
r	radius
T	absolute temperature
V	volume
z	charge
γ	activity coefficient
ϵ_0	permittivity of the vacuum
ϵ_α	relative permittivity of the phase α
ϕ^o	inner potential of the oil phase
ϕ^w	inner potential of the aqueous phase
$\Delta_o^w \phi$	Galvani potential difference
$\Delta_o^w \phi_i^0$	Standard potential of transfer for ion i
$\Delta_o^w \phi_i^{0'}$	formal potential of transfer for ion i

$\Delta_o^w \phi_{1/2}$	half-wave potential
$\Delta_o^w \phi_{ET}^0$	standard redox potential for the interfacial electron transfer
$\mu_i^{0,\alpha}$	standard chemical potential of i in phase α
$\tilde{\mu}_i^\alpha$	electrochemical potential of ion i in phase α
v	scan rate
η	viscosity

Subscripts:

0	initial value
i	species i
p	peak

Superscripts:

0	standard value
o	oil phase
w	aqueous phase
α	phase α

List of Abbreviations

BA ⁺	bis(triphenylphosphoranylidene) ammonium
CcO	Cytochrome <i>c</i> oxidase
CE	counter electrode
Co ₂ (DPOx)	biscobaltporphyrin of 2,2'-bis[5-(2,8,13,17-tetraethyl-3,7,12,18-tetramethylporphyrinyl)] diphenylether
Co ₂ (DPO)	biscobaltporphyrin of 4,6-bis[5-(2,8,13,17-tetraethyl-3,7,12,18-tetramethylporphyrinyl)] dibenzofuran
Co ₂ (DPX)	biscobaltporphyrin of 4,5-bis[5-(2,8,13,17-tetraethyl-3,7,12,18-tetramethylporphyrinyl)]-9,9-dimethylxanthene
CoAP	cobalt(II) 2,8,13,17-tetraethyl-3,7,12,18-tetramethyl-5-p-aminophenylporphyrin
CoOEP	2,3,7,8,12,13,17,18-octaethylporphyrin cobalt
CoP	cobalt porphine
CoPc	cobalt phthalocyanine
CoTPP	5,10,15,20-meso-tetraphenylporphyrin cobalt
CV	cyclic voltammetry or voltammogram
D	electron donor
DcMFC	decamethylferrocene
DCB	1,2-dichlorobenzene
DCE	1,2-dichloroethane
DFcE	1,2-diferrocenylethane
DFT	density functional theory
DMFc	1,1'-dimethylferrocene
ET	electron transfer
ESI-MS	electrospray ionization mass spectrometry
Fc	ferrocene
FcCOOH	ferrocene carboxylic acid
FcMeOH	ferrocene methanol
H ₂ FAP	free-base 2,8,13,17-tetraethyl-3,7,12,18-tetramethyl-5-p-aminophenylporphyrin
IT	ion transfer
ITIES	Interface between two immiscible electrolyte solutions
L	ligand
M	metal; mediator

MS	mass spectrometry
NADH	nicotinamide adenine dinucleotide
O	oxidized species
o	oil phase
ORR	oxygen reduction reaction
PCET	proton-coupled electron transfer
PTC	phase transfer catalysis or catalyst
PTFE	polytetrafluoroethylene
PVC	polyvinylchloride
R	reduced species
RE	reference electrode
RTIL	room temperature ionic liquid
SECM	scanning electrochemical microscopy
SHE	standard hydrogen electrode
TB ⁻	tetrakis(pentafluorophenyl)borate
TEA ⁺	tetraethylammonium
TiO _x	titanium oxalate
TPB ⁻	tetraphenylborate
TPAs ⁺	tetraphenylarsenium
TTF	tetrathiafulvalene
UV-Vis	ultraviolet-visible
UME	ultramicroelectrode
w	water

1 Introduction

Studies of electrochemistry at the interface between two immiscible electrolyte solutions (ITIES) is a relatively new field of contemporary electrochemistry, dating back to the works of Gavach *et al.* in France¹⁻⁴ and Koryta and Samec *et al.* in Prague⁵⁻⁹ in the 1970s. This field has evolved significantly, becoming a truly versatile area with applications including solvent extraction, separation, phase-transfer catalysis, photochemistry, and biomembrane studies.^V In recent years electrochemical studies at liquid-liquid interfaces have experienced renewed interest because they offer well reproducible, defect free platforms to study electrocatalysis of many important reactions like oxygen and carbon dioxide reduction or hydrogen evolution.¹⁰ These reactions can be considered as proton-coupled electron transfer reactions, indicating that they have a reaction step where both proton and electron are transferred simultaneously. They also require efficient catalysts to lower the activation energy and enhance the rate of the reaction.

Studies of these fundamental energy related reactions are important in order to find alternatives to the current hydrocarbon economy to convert and store energy.¹¹ In order to do this we need efficient ways to store the energy in fuels (for example hydrogen or ethanol) and to liberate the stored energy. One method to utilise the stored energy is to oxidize the fuels with oxygen either by burning (releasing the energy as heat) or by electrochemical oxidation of the fuel and reduction of oxygen with a fuel cell to convert the chemical energy directly into electricity. For example, solar energy could be stored by producing hydrogen, which could then be oxidized in a fuel cell when electricity is needed. As oxygen reduction is one of the main sources of energy loss, we would need to improve the efficiency of oxygen reduction to minimise the energy losses when converting the fuel to produce energy. Improving our understanding of the oxygen reduction mechanism and electrocatalysis of that reaction is one of the main focuses of this thesis.

To date, platinum and platinum alloys are the best available options to catalyse oxygen reduction, but due to the high price of these precious metals, alternative catalysts would be beneficial. One approach is to mimic nature: oxygen reduction in the cell respiration chain is catalysed by an enzyme, cytochrome *c* oxidase (CcO), bound in the hydrophobic lipid bilayer of the mitochondrial membrane. The active centre of CcO consists of an iron porphyrin/copper heterodinuclear centre, where a copper atom coordinated by three histidines is located above the iron centre of the heme.^{12,13} Porphyrins and different organometallic

compounds with bimetallic active sites are therefore possible candidates as non-noble metal electrocatalysts to be utilised in fuel cells. Electrochemistry at liquid-liquid interfaces offers an excellent way to study both the catalytic activity and the selectivity of these catalysts.¹¹ In fact, the analogy with biological cell membranes, where the hydrophobic tails of the phospholipids form an oil phase, and the water-oil-water system was pointed out by Cremer as early as 1906.¹⁴

This thesis gives an introduction to electrochemistry at liquid-liquid interfaces, from the structure of the interface to different charge transfer processes occurring at the ITIES (**Publication V**). A brief introduction to proton-coupled electron transfer (PCET) is given, followed by a summary of the earlier work of oxygen reduction at ITIES. Oxygen reduction at the liquid-liquid interface by 1,2-diferrocenyethane was studied in order to gain more information about how the reaction occurs with metallocenes (**Publication I**). Also reduction of hydrogen peroxide, a product of two-electron reduction of molecular oxygen, was studied. Surprisingly, reduction of hydrogen peroxide was found to be faster than oxygen reduction.

Oxygen reduction at ITIES can be catalysed by nanoparticles or molecular catalysts.¹⁰ In order to achieve selective four-electron reduction of molecular oxygen to water, cofacial biscobalt porphyrins with the structure mimicking the active centre of CcO were studied as catalysts at ITIES (**Publication II**). In order to elucidate the effects of the transition metal containing redox mediators to the observed yield of hydrogen peroxide, two mediators of similar reducing ability, 1,1'-dimethylferrocene and tetrathiafulvalene, were used. The results showed that all the catalysts produced both hydrogen peroxide and water, contradicting the previous results. The unexpected hydrogen peroxide production was attributed to the oxygen reduction taking place at the “exo” side of the porphyrin, when the selective four-electron reduction to water was attributed to the reaction at the “endo” side of the catalyst, and a new “dock-on/dock-in” mechanism was proposed to explain these results. In order to utilise the oxygen reduction at ITIES in practical applications, a novel fuel cell with the oxygen reduction catalysed by a molecular catalyst taking place at the liquid-liquid interface was demonstrated in **Publication IV**.

Another type of catalysis involving liquid-liquid interfaces is phase-transfer catalysis, where a biphasic reaction with reactants in different phases is driven by the addition of a catalyst, typically a quaternary ammonium salt.¹⁵⁻¹⁷ The ammonium salt extracts one of the reactants across the interface, allowing the reaction to take place. In this thesis we also demonstrated a

slightly similar method wherein the acid catalysed synthesis of organic chemicals is performed at the ITIES by utilising proton transfer catalysis. The protons transferred electrochemically or chemically across the liquid-liquid interface were shown to be able to catalyse S_N1 substitution of indole to ferrocene methanol (**Publication III**). This is a novel way to utilise electrochemistry at ITIES for organic synthesis.

In summary, this thesis presents how electrochemistry at the ITIES can be utilised in catalysis and electrocatalysis research, and describes some practical applications where the methodologies could be utilised. The scope of the thesis is the utilisation of proton transfer across the ITIES to perform oxygen reduction (either catalysed or non-catalysed) or to catalyse S_N1 substitutions of indole to ferrocene methanol. Oxygen reduction was studied both in an electrochemical cell (**Publications I and II**) and in a fuel cell (**Publication IV**). This thesis confirms that electrochemistry at liquid-liquid interfaces is a versatile field with promising and interesting applications, and should not be ignored as a niche field without any future.

2 Electrochemistry at Liquid-Liquid Interfaces

2.1 Interface between Two Immiscible Electrolyte Solutions

The study of charge transfer processes across interfaces between immiscible solutions dates back to the early work of Nernst and Riesenfeld, who described the transfer of potassium iodide between two aqueous phases separated by phenol phase in 1902.¹⁸ However, studies in the following years concentrated mostly on distribution measurements of salts between two immiscible phases.¹⁹ The field of electrochemistry at the interface between two immiscible electrolyte solutions (ITIES) gained more momentum in the 1970s with the pioneering work of Gavach *et al.* in France¹⁻⁴ and Koryta *et al.* in Prague⁵⁻⁹, demonstrating that the ITIES could be polarized like a conventional electrode-electrolyte interface. This enabled the use of common electrochemical techniques to study charge transfer reactions at the ITIES. The modern era of electrochemistry at ITIES began with the four-electrode potentiostat with positive feedback ohmic drop compensation, introduced by Samec *et al.* in 1977,^{5,20,21} as now the Galvani potential difference could be accurately controlled with the help of the two reference electrodes and the effects of low conductivity in the oil phase could be eliminated. Consequently, the conventional electrochemical techniques developed for solid electrodes, like cyclic voltammetry,^{20,21} chronoamperometry,²² polarography,²³ differential pulse stripping voltammetry,²⁴ alternating current voltammetry²⁵ and impedance²⁶ could now be applied to study charge transfer across liquid-liquid interfaces.

Most publications have reported mainly experimental results,²⁷⁻²⁹ but in comparison only few theoretical models of charge-transfer processes and of the interfacial structure have been proposed.^{30,31} Although the potential distribution at the ITIES is now well established,³² the structure of the interface and the kinetics of transfer are still controversial subjects.^{30,31,33}

2.2 Structure of the Liquid-Liquid Interface

The Galvani potential difference, $\Delta_o^w\phi$, across the interface is defined as the difference between the potential of the bulk aqueous phase ϕ^w and the potential of the bulk oil phase ϕ^o . The potential distribution at the interface has classically been described by two back-to-back Gouy-Chapman layers (Verwey-Niessen model), where the electric potential decreases exponentially away from the interface.³⁴ The model was later modified to take into account

the Stern layer (Modified Verwey-Niessen), the layer of ions specifically adsorbed on the surface.³⁵ Girault and Schiffrin proposed a mixed solvent layer, where ions from one phase could penetrate into the mixed region and form ion pairs with the counter ions of the opposite phase.³⁶ This model was supported by theoretical calculations based on the lattice gas model^{37,38} and experimental results obtained with ellipsometry,³⁹ but the molecular dynamics simulations showed instead a sharp but rough interface with the finger like solvent groups penetrating into the opposing phase on a pico-second time scale.⁴⁰⁻⁴² The thickness of the layer where these fluctuations are observed was calculated to be *ca.* 10 Å at the water-1,2-dichloroethane (w-DCE) interface, and the calculations were confirmed experimentally by neutron reflectivity.⁴³ Hence the interface can be considered sharp on a molecular level, but on average it is a region where the two solvents mix. Snapshots from molecular dynamics computer simulations show that the local structure of the interface is greatly influenced by the presence of ionic charges,³⁰ as shown by studies of distribution of ions at an electrified ITIES by x-ray reflectivity at the water-nitrobenzene^{44,45} and w-DCE⁴⁶ interfaces. The results show clearly the failure of the Gouy-Chapman theory at large Galvani potential differences perhaps indicating that the interface becomes less ideally polarized. Instead, an ion specific Poisson-Boltzmann equation incorporating a potential of mean force for each ion to account for the variation of solvation in the interfacial region agreed excellently with the experimental results. The structure of the liquid-liquid interface has been thoroughly discussed in the recent review by Dryfe.³⁰

Numerous efforts have been made to reach a better understanding of the molecular mechanisms involved in ionic motion in liquids and ion transfer across ITIES,^{30,47,48} and results suggest that the rate-limiting step of ion transport is the necessary interchange of the solvation shell from one liquid to the other. The roughness of the interface is likely to manifest itself as capillaries or fingers of one liquid protruding into another.^{49,50} These protrusions resulting from the long-range ion-dipole interactions plays a major role in the change of the solvation shell,⁵¹ implying that ion transfer (IT) may be an activated process.⁵² This has been corroborated by molecular dynamics calculations as described earlier.^{38,51} From an experimental viewpoint, the majority of the charge-transfer reactions studied are reversible (*i.e.* kinetically fast) and the development of their applications is not hindered by these theoretical limitations.

2.3 Thermodynamics of the ITIES

The standard Gibbs free energy to transfer an ion i from the aqueous to the oil phase ($\Delta G_{tr,i}^{w \rightarrow o}$) can be related to the standard potential of ion transfer, $\Delta_o^w \phi_i^0$, by Equation 1.

$$\Delta_o^w \phi_i^0 = \frac{\Delta G_{tr,i}^{w \rightarrow o}}{z_i F} = \frac{\mu_i^{0,o} - \mu_i^{0,w}}{z_i F} \quad (1)$$

where $\mu_i^{0,\alpha}$ is the standard chemical potential of i in either phase ($\alpha = o$ or w), z_i is the charge of i , and F is the Faraday constant. Hence the distribution of the species at the interface is given by the Nernst-Donnan equation for ITIES (analogous with metal electrodes):

$$\phi^w - \phi^o = \Delta_o^w \phi = \Delta_o^w \phi_i^0 + \frac{RT}{z_i F} \ln \frac{a_i^o}{a_i^w} = \Delta_o^w \phi_i^{0'} + \frac{RT}{z_i F} \ln \frac{c_i^o}{c_i^w} \quad (2)$$

where $\Delta_o^w \phi_i^{0'}$ is the formal potential of ion transfer for species i from water to oil, R is the molar gas constant, T is the temperature and a_i and c_i are the activity and concentration of species i , respectively.

The determination of a transfer potential of an ion requires an extra thermodynamic assumption. The most commonly used is the TATB hypothesis, which states that the transfer energy of tetraphenyl borate and tetraphenylarsenium are equal between any pair of solvents⁵³ (*i.e.* by choosing that $\Delta_o^w \phi_{TPAs^+}^0 = -\Delta_o^w \phi_{TPB^-}^0$ independent of the solvent). This assumption is partly justified as the size of the molecule is not affected greatly by the centre atom and the charge is shielded by the bulky phenyl rings. However, molecular dynamics simulations of two spherical big oppositely charged ions show that this assumption has some limitations: water interacts more strongly with negative ions while positive ions are better solvated by organic solvents (for example acetonitrile or chloroform).⁵⁴ The $\Delta G_{tr,i}^{w \rightarrow o}$ values depend on the organic solvent, but it has been observed experimentally that there is a linear correlation between the $\Delta G_{tr,i}^{w \rightarrow o}$ values determined for different solvents. Hence this correlation can be used to estimate transfer energies when experimental data is not available.⁵⁵⁻⁵⁷

Equation 2 has two significant meanings: the distribution of species can be controlled by controlling the Galvani potential difference across the interface, and the Galvani potential difference can be adjusted by the distribution of species between the phases. Naturally, the electroneutrality condition has to be fulfilled in both phases. If the electrolytes are not significantly partitioning between the phases, the interface behaves as an ideally polarisable electrode: the potential across the interface can be varied significantly without any current. The potential region where the interface behaves as a polarisable electrode is called the potential window. When the aqueous phase is made very positive compared to the oil phase, either a cation in the aqueous phase (for example Li^+ or H^+) transfers into the oil phase, or an anion transfers from the oil phase to the aqueous phase. Ion transfer across the interface is observed as electric current, with the positive sign assigned to the transfer of positive charge from the aqueous to the oil phase. The process taking place depends on the standard potentials of ion transfer: for example tetraphenyl borate (TPB⁻) transfers before lithium and therefore determines the positive limit of the potential window.²⁷ If both phases contain species that partition between the phases, the Galvani potential difference is adjusted by the partition of the common ions. Now the interface can be treated as an ideal non-polarisable electrode: even a small change in the potential causes the common ion to transfer across the interface.^{27,58} These two cases are illustrated in Figure 1.

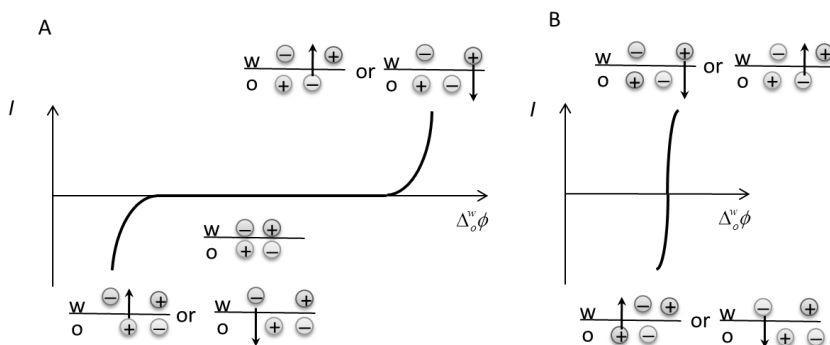


Figure 1. Current-voltage characteristics of a polarisable (A) and non-polarisable (B) interface.^{IV}

In a system where ionic species of the two immiscible liquid phases are in equilibrium the potential difference across the interface can be calculated with the Nernst equation (Eq. 2) and taking into account mass balance equations.⁵⁸ The mass balance for species i is

$$n_{i, \text{total}} = n_i^o + n_i^w \quad (3)$$

$$V^o c_{i,\text{initial}}^o + V^w c_{i,\text{initial}}^w = V^o c_i^o + V^w c_i^w \quad (4)$$

Additionally, the electroneutrality condition of both phases must be fulfilled:

$$\sum_i z_i c_i^w = \sum_i z_i c_i^o = 0 \quad (5)$$

Combination of Equations 3-5 gives

$$\sum_i z_i \frac{V^o c_{i,\text{initial}}^o + V^w c_{i,\text{initial}}^w}{V^w + V^o \exp\left[\frac{zF}{RT} (\Delta_o^w \phi - \Delta_o^w \phi_i^o)\right]} = 0 \quad (6)$$

Equation 6 can be solved numerically to evaluate the Galvani potential difference of the system in equilibrium, and Nernst equation and mass balance equations can be used to calculate the compositions of both phases.

2.4 Charge Transfer at the Liquid-Liquid Interface

2.4.1 Ion Transfer at the Liquid-Liquid Interface

Ion transfer is one of the simplest charge transfer reactions at a liquid-liquid interface. By applying an external potential across the interface, ions in both phases move across the interface until the Nernst equation is fulfilled. The transfer of ions across the interface is observed as an electric current, and electroneutrality is maintained by electrode reactions at the counter electrodes. Figure 2 shows a typical ion transfer voltammogram of the water-1,2-dichlorobenzene (DCB) system. The aqueous phase contains 10 mM HCl and DCB contains 5 mM bis(triphenylphosphoranylidene) ammonium tetrakis(pentafluorophenyl) borate (BATB) to guarantee the sufficient electric conductivity.

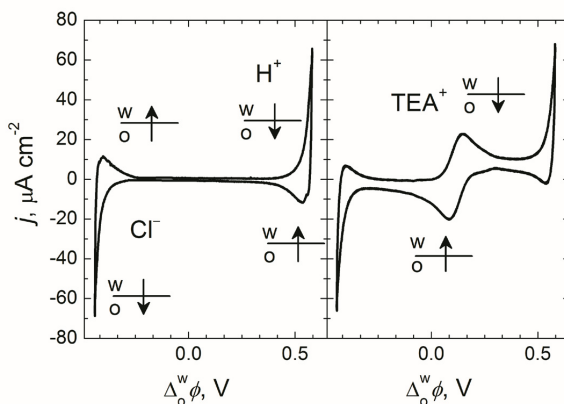


Figure 2. Cyclic voltammogram of the interface between 10 mM HCl (aq) and 5 mM BATB (DCB) without (left) and with addition of a small amount of TEACl in the aqueous phase (right). Scan rate of 50 mV s^{-1} .¹⁹

When the Galvani potential difference across the interface is made more positive, proton transfer from the aqueous to the oil phase takes place at the positive limit of the potential window. When the scan direction is switched at 0.55 V, protons in the oil phase transfer back to the aqueous phase, seen as a negative diffusion limited current peak. Similarly, the reversible transfer of chloride from the aqueous phase to the DCB phase is observed at the negative limit of the potential window. Only a small current due to charging of the electrical double layers of the interface is observed in the middle of the window. When a small amount of tetraethylammonium chloride (TEACl) is added to the aqueous phase, the transfer of TEA^+ is observed in the middle of the window as a voltammetric wave, because its standard transfer potential is low compared to the potentials of the supporting electrolytes. This is a typical example of simple ion transfer, and it is analogous with a simple mass transport limited reversible electron transfer reaction at an electrode-electrolyte interface. The mass transport limited shape of the voltammogram for TEA^+ transfer is now due to the depletion of the ion on the one side of the interface. From a practical point of view the transfer of ions is very fast with the rate constant of *ca.* $0.5\text{-}1 \text{ cm s}^{-1}$,³¹ and thus ion transfer reactions at the ITIES can be considered reversible. Thus, the peak potentials are independent of the scan rate and have a the peak separation of $59/z_i \text{ mV}$ at $25 \text{ }^\circ\text{C}$. Also the Randles-Ševčík equation for the peak-current i_p is valid for reversible ion transfer.⁵⁹

$$i_p = 0.4463 z_i A F c_{i,0} \sqrt{\frac{z_i F}{RT}} \sqrt{v} \sqrt{D_i} \quad (7)$$

where A is the area of the interface, $c_{i,0}$ is the initial concentration of the transferring species, ν is the scan rate and D_i is the diffusion coefficient of the species in the phase from where it is transferring. Cyclic voltammetry can also be used to determine the standard potential of transfer for the species transferring in the middle of the potential window from the observed half-wave potential. The condition for half-wave potential at the interface is⁵⁹

$$D_i^{w/2} c_i^w = D_i^{o/2} c_i^o \quad (8)$$

Thus, from Equation 2 for ion transfer we get:

$$\Delta_o^w \phi_{1/2} = \Delta_o^w \phi_i^0 + \frac{RT}{z_i F} \ln \frac{\gamma_i^o}{\gamma_i^w} - \frac{RT}{z_i F} \ln \sqrt{\frac{D_i^o}{D_i^w}} = \Delta_o^w \phi_i^{0'} - \frac{RT}{z_i F} \ln \sqrt{\frac{D_i^o}{D_i^w}} \quad (9)$$

In some cases the diffusion coefficients of the species in the oil phase are difficult to determine experimentally, so they can be estimated instead with Walden's rule,⁶⁰ stating that

$$\frac{D_i^o}{D_i^w} = \frac{\eta^w}{\eta^o} \quad (10)$$

However, this relation is not completely accurate for ions in aqueous solvents due to strong hydration. The activity coefficients in Equation 9 can be estimated for example with the Debye-Hückel theory.⁶¹ This methodology can also be utilised to calculate the partition coefficients of charged drugs between the aqueous and oil phase:

$$P_i = \frac{a_i^o}{a_i^w} = \exp\left[\frac{z_i F}{RT} (\Delta_o^w \phi - \Delta_o^w \phi_i^0)\right] = P_i^0 \exp\left[\frac{z_i F}{RT} (\Delta_o^w \phi)\right] \quad (11)$$

$$P_i^0 = \exp\left[-\frac{z_i F}{RT} \Delta_o^w \phi_i^0\right] \quad (12)$$

The transfer energy of the neutral species can be estimated by subtracting the charge dependent part of the transfer energy (Eq. 13).⁶² This can be calculated for example with the theoretical model of Born (Eq. 14) or Abraham-Liszi, or with the semiempirical model by Osakai *et al.*⁶²

$$\Delta G_{\text{tr,neutral}}^{\text{w} \rightarrow \text{o}} = \Delta G_{\text{tr,ion}}^{\text{w} \rightarrow \text{o}} - \Delta G_{\text{tr}}^{\text{w} \rightarrow \text{o}} \text{ (charge dependent)} \quad (13)$$

$$\Delta G_{\text{tr}}^{\text{w} \rightarrow \text{o}} \text{ (charge dependent)} = \frac{N_{\text{A}} e^2}{8\pi\epsilon_0 r} \left(\frac{1}{\epsilon_0} - \frac{1}{\epsilon_{\text{w}}} \right) \quad (14)$$

where N_{A} is Avogadro's constant, e is the elementary charge, r is the radius of the ion, ϵ_0 is the permittivity of vacuum, and ϵ_{w} and ϵ_0 are the relative permittivity of the aqueous and the oil phase, respectively.

The determination of the standard potential of transfer for the species limiting the potential window is not as straightforward as described by Equation 9, as the half-wave potential cannot be determined directly. Hence special methods developed for this problem based on convolution integrals are used.⁶³

2.4.2 Facilitated Ion Transfer at the Liquid-Liquid Interface

If an ion forms a complex with a neutral species in the oil phase, complexation can lower the transfer energy and thus the transfer potential. This phenomenon was first observed by Koryta in 1979, who reported the facilitated transfer of potassium and sodium from the aqueous phase by the dibenzo-18-crown-6 polyether in the oil phase.⁶ The facilitated transfer of these very hydrophilic ions was observed as diffusion limited peak in the middle of the potential window, while alkali metal cations normally transfer at the positive limit of the window. The shapes of the peaks are typical to diffusion limited processes resulting from the mass transport limitation of the complexing species. If the ligand forms a simple 1:1 complex, the equilibrium constant K_{a} for the complexation of the transferring ion M^z with the ligand L is simply

$$K_{\text{a}} = \frac{a_{\text{ML}^z}^{\text{o}}}{a_{\text{L}}^{\text{o}} a_{\text{M}^z}^{\text{o}}} \quad (15)$$

The half-wave potential for the observed facilitated ion transfer ($c_{\text{M}^z}^{\text{w}} \gg c_{\text{L}}^{\text{o}}$)⁷ can be expressed as

$$\Delta_o^w \phi_{1/2} = \Delta_o^w \phi_i^{0'} - \frac{RT}{z_i F} \ln \sqrt{\frac{D_{ML}^o}{D_L^o}} - \frac{RT}{z_i F} \ln(K_a c_{M^z}^w) \quad (16)$$

This equation states that stronger complexation and higher concentration of the transferring ion causes a larger shift of the half wave potential (and, in the same way, of the peak potential) to more negative potentials for cations (and more positive potentials for anions).

Simple ion transfer from an aqueous to an oil phase can also be treated as a facilitated transfer by the counter ion of the supporting electrolyte in the oil phase. Recent measurements with liquid-liquid interfaces supported on nanopipettes show that the transfer of most cations and some anions is facilitated by the hydrophobic counter ion at the interface by ion-pair formation.⁶⁴ However, the association constants are generally very low, leading to the dissociation of the ion pair in the bulk phase. Ion transfer can thus be described as a shuttling mechanism where the counter ion carries the transferring species across the mixed layer to the bulk phase.⁶⁴ It was also observed that trace amounts of water in the organic solvent had a crucial effect on the transfer of hydrophilic ions: no transfer of alkali metal cations was observed into dry DCE even at a polarisation of more than 2 V, but the transfer into DCE saturated with water (130 mM) took place at 0.5 V. A more hydrophobic tetramethylammonium cation was unaffected by the water concentration. Hence the transfer of alkali metal cations is facilitated by the water clusters present in DCE.⁶⁵

2.4.3 Electron Transfer at the Liquid-Liquid Interface

Heterogeneous electron transfer (ET) across the liquid-liquid interface can take place between two redox couples located in different phases (for example ET between aqueous ferri-ferrocyanide and ferrocenium-ferrocene in the oil phase).⁶⁶ The ET reaction can be controlled with the Galvani potential difference. If we consider the Reaction i at equilibrium:



$$\tilde{\mu}_{O_1}^w + \tilde{\mu}_{R_2}^o = \tilde{\mu}_{R_1}^w + \tilde{\mu}_{O_2}^o \quad (17)$$

we can write the Nernst equation for the ET reaction:

$$\Delta_{\circ}^w \phi = \Delta_{\circ}^w \phi_{\text{ET}}^0 + \frac{RT}{F} \ln \frac{a_{\text{R}_1}^w a_{\text{O}_2}^{\circ}}{a_{\text{O}_1}^w a_{\text{R}_2}^{\circ}} \quad (18)$$

where $\Delta_{\circ}^w \phi_{\text{ET}}^0$ is the standard redox potential for the interfacial transfer of electrons, the difference of the standard redox potentials of the redox couples expressed on the same reference scale, usually aqueous Standard Hydrogen Electrode (SHE).

$$\Delta_{\circ}^w \phi_{\text{ET}}^0 = [E_{\text{O}_2/\text{R}_2}^0]_{\text{SHE}}^{\circ} - [E_{\text{O}_1/\text{R}_1}^0]_{\text{SHE}}^w \quad (19)$$

Electron transfer at the liquid-liquid interface has one fundamental difference compared to the solid-liquid interface. At a solid-liquid interface the degree of freedom is one, as the system is fully characterized by the concentrations of the redox species O and R and the electrode potential. In this case there are two restricting conditions: mass balance equation and the Nernst equation. But in a liquid-liquid system there are five parameters, as shown in Equation 18, concentrations of the four redox species and the Galvani potential difference, while the system is restricted by mass balance equations in both phases (Reaction i) and the Nernst equation (Eq. 18). Hence, the degree of freedom in a liquid-liquid system is two, and now it is possible to vary two parameters independently.⁶⁶

The redox potentials of organic redox couples can be evaluated with thermodynamic cycles, or the redox potential can be determined on the ferrocene scale, as this redox potential in DCE has been evaluated previously with the thermodynamic cycle.¹⁰

$$[E_{\text{Fc}^+/\text{Fc}}^0]_{\text{SHE}}^{\circ} = 0.64 \pm 0.05 \text{ V} \quad (20)$$

Another method is to determine the standard redox potential for the interfacial transfer of electrons with a species of known redox potential, like ferri-ferrocyanide, using Equations 18 and 19. Because the standard redox potential in water is usually known, it is possible to evaluate the corresponding redox potential in an oil phase. The redox potential in the organic solvent vs. aqueous SHE for a general n electron reduction of species O to R can be calculated from the thermodynamic cycle if the Gibbs energies of transfer between water and the solvent for R and O are known.⁶⁷

$$\begin{aligned} [E_{\text{O/R}}^0]_{\text{SHE}}^{\alpha} &= [E_{\text{O/R}}^0]_{\text{SHE}}^{\text{w}} + \frac{1}{nF}(\mu_{\text{O}}^{\circ,\alpha} - \mu_{\text{R}}^{\circ,\alpha} - \mu_{\text{O}}^{\circ,\text{w}} + \mu_{\text{R}}^{\circ,\text{w}}) = \\ & [E_{\text{O/R}}^0]_{\text{SHE}}^{\text{w}} + \frac{1}{nF}(\Delta_{\alpha}^{\text{w}}G_{\text{O}}^0 - \Delta_{\alpha}^{\text{w}}G_{\text{R}}^0) \end{aligned} \quad (21)$$

where $\Delta_{\alpha}^{\text{w}}G_i^0$ is the Gibbs energy of transfer of the species i from aqueous phase to phase α . Hence the redox potential for hydrogen evolution in an oil phase can be expressed as⁶⁸

$$[E_{\text{H}^+/\text{H}_2}^0]_{\text{SHE}}^{\text{o}} = [E_{\text{H}^+/\text{H}_2}^0]_{\text{SHE}}^{\text{w}} - \frac{(\Delta G_{\text{tr,H}_2}^{\text{w}\rightarrow\text{o}} - 2\Delta G_{\text{tr,H}^+}^{\text{w}\rightarrow\text{o}})}{2F} \quad (22)$$

It can be seen from Equation 21 that the reaction shifts to higher potentials if the transfer of O from water to phase α is unfavourable ($\Delta_{\alpha}^{\text{w}}G_{\text{O}}^0 > 0$) and the transfer of R is thermodynamically favourable ($\Delta_{\alpha}^{\text{w}}G_{\text{R}}^0 < 0$). For example, transfer energy of protons from water to DCE is 53 kJ mol⁻¹⁶⁹ and the corresponding transfer energy of hydrogen is -2.6 kJ mol⁻¹⁷⁰. The transfer energy of hydrogen is almost negligible, as most of the contribution comes from the transfer of protons into the oil phase. Thus a value of $[E_{\text{H}^+/\text{H}_2}^0]_{\text{SHE}}^{\text{DCE}} = 0.55$ V has been estimated.⁶⁸ This indicates that hydrogen evolution is considerably easier in DCE, but extra energy is needed to transfer the protons into the oil phase. Redox reactions taking place in different solvents have different redox potentials, as shown in the figure below for some redox reaction in water and DCE.

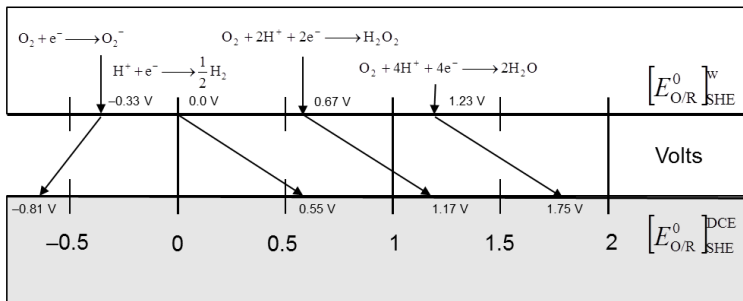


Figure 3. Redox potential scale for oxygen in water (top scale) and in 1,2-dichloroethane (bottom scale) versus the aqueous Standard Hydrogen Electrode (SHE). Adapted from Ref. 10.

2.4.4 Photoinduced Charge Transfer at Liquid-Liquid Interfaces

From the early days, liquid-liquid interfaces have been considered as biomimetic models of biomembranes,¹⁴ and some work has been dedicated to study photo-induced reactions with the long-term goal to study and understand artificial photosynthesis. For example, Kotov and Kuzmin have studied the transfer of photogenerated ions across the ITIES.⁷¹ It was also quickly realized that it was possible to study photo-induced electron transfer reactions between an excited sensitizer in one phase and a redox quencher in the adjacent phase. The advantage of this system is that as the sensitizer and quencher are located in different phases, the recombination reaction becomes more unfavourable. Fermin *et al.* published a series of papers to characterize the different steps of those photo-induced processes (see for example part VII⁷²). A good level of understanding was reached and an analytical model to describe the photo-induced ET was developed.⁷³ More recently, it has been shown that gold nanoparticles adsorbed at the ITIES could enhance these photo-induced ET reactions due to a surface plasmon resonance effect of the nanoparticles.⁷⁴

3 Experimental Procedures

3.1 Four-Electrode Cell Experiments

All of the electrochemical measurements described in this work were performed at ambient temperature (20 ± 2 °C) in a Faraday cage. For anaerobic conditions, the measurements were done in a nitrogen glove box. Cyclic voltammograms (CVs) at the liquid-liquid interface were recorded with an Autolab four-electrode potentiostat PGSTAT100 (EcoChemie, the Netherlands) at the scan rate of 50 mV s^{-1} . A glass cell shown in Figure 4 designed for liquid-liquid interface experiments with an interfacial area of 0.159 cm^2 was a generous gift from professor Zdeněk Samec, J. Heyrovský Institute of Physical Chemistry, Prague.

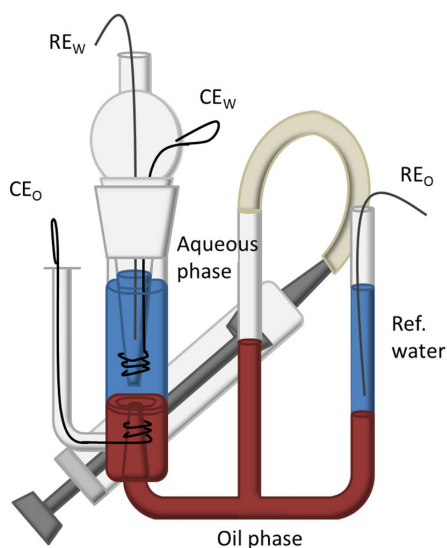


Figure 4. Four-electrode cell for ITIES studies.^{III}

Two reference electrodes (RE, Ag/AgCl), placed in Luggin capillaries to reduce iR drop, controlled the potential difference across the interface, while the tungsten counter electrodes (CE) in both phases provided electric current. The organic reference phase had a common cation with the supporting electrolyte of the organic phase, establishing a stable distribution potential at the ref. water-oil interface according to Equation 2. This interface can be considered as non-polarisable (see Figure 1). The measured potential was converted to the Galvani potential scale based on cyclic voltammetry measurement of the reversible half-wave potential of TEA^+ transfer. Almost all the potential drop can be considered to occur at the

ITIES as positive feedback *iR* compensation was utilised to eliminate the effect of the low conductivity of the oil phase.

The available potential window at the ITIES is limited by the supporting electrolytes. To widen the potential window, highly hydrophobic salts should be used as supporting electrolytes in the oil phase. One of the most commonly used salt is bis(triphenylphosphoranylidene) ammonium tetrakis(pentafluorophenyl) borate (BATB, see Figure 5), as it is hydrophobic enough that the potential window is limited by the transfer of species from the aqueous phase. Typically the organic supporting electrolytes are prepared by the metathesis of stoichiometric amounts of chloride and lithium salts of the ions (for example BACl and LiTB) dissolved in 2:1 mixture of methanol and water. The resulting precipitate is recrystallized from 1:1 mixture of acetone and ethanol and washed with the 2:1 mixture of methanol and water to remove the residues of the starting materials.

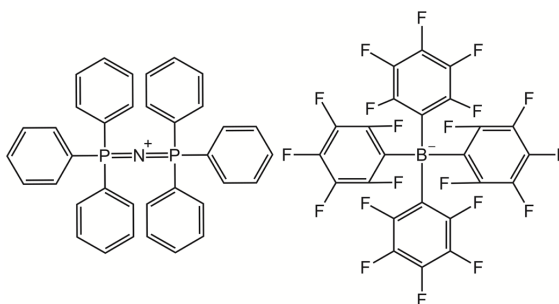
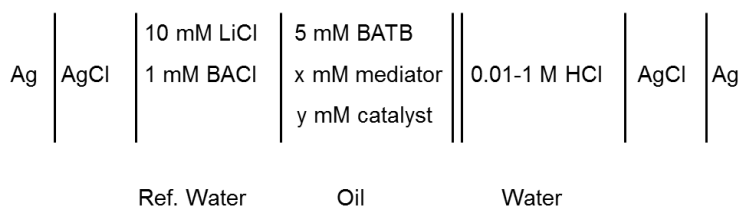


Figure 5. Bis(triphenylphosphoranylidene) ammonium tetrakis(pentafluorophenyl) borate

Most commonly used solvents are nitrobenzene, 1,2-dichloroethane, and *o*-nitrophenyl octyl ether. All the reported systems until 2011 have been recently listed.^{28,29} Very recently Olaya et al. have shown that trifluorotoluene is a good solvent immiscible with water, with a reasonably high dielectric constant and lesser toxicity than DCE.⁵⁷ There has also been growing interest in interface between water and ionic liquids (RTIL),⁷⁵ as RTILs have negligible volatility, reasonable conductivity and unique solvation properties. However, they suffer from high viscosity, leading to a lower mass transport rate. The width of the potential window depends on the solubility of the ionic liquid in water, but by a choice of suitable ions a potential window comparable to the water-DCE system has been achieved.⁷⁵ Suitability of a series of chlorinated solvents for electrochemistry at the ITIES has been studied in terms of the width of the potential window and required *iR* compensation.^{IV} DCE and DCB were chosen as solvents for this work, as they display wide potential window and reasonable ohmic losses. Typical cell composition is shown in Scheme 1.



Scheme 1. The typical electrochemical cell composition for the four-electrode cell experiments.

Mediator is a molecule that can be oxidized in the reaction: for example ferrocene (Fc), 1,1'-dimethylferrocene (DMFc), decamethylferrocene (DeMFC), 1,2-diferrocenylethane (DFcE), and tetrathiafulvalene (TTF) have been used in this work. Structures of some of the mediators are shown in Figure 6.

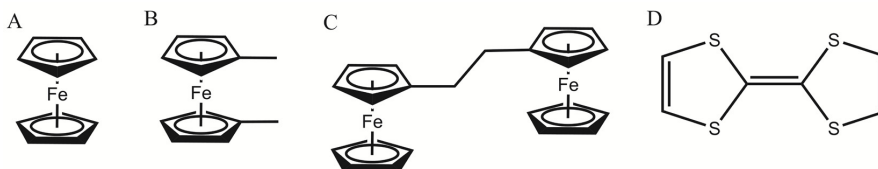


Figure 6. Molecular structures of ferrocene (A), 1,1'-dimethylferrocene (B), 1,2-diferrocenylethane (C), and tetrathiafulvalene (D).

3.2 Two-Phase Reactions with Chemically Controlled Polarisation

As described in Section 2.3, the polarisation of the ITIES can also be controlled chemically in a shake-flask experiment by addition of ions partitioning between both phases and establishing a distribution potential according to the Nernst-Donnan equation (Eq. 2). For example, to achieve proton transfer into the oil phase, LiTB can be added into the aqueous phase. Highly hydrophobic TB^- will transfer into the oil phase with an equal amount of protons to maintain electroneutrality, and now the Galvani potential difference and composition of both phases can be calculated as described in Section 2.3. Typical cell composition for the shake-flask experiments is shown in Scheme 2.

5 mM BATB		5 mM LiTB
x mM mediator		10 mM HCl
y μ M catalyst		
Oil		Water

Scheme 2. The typical electrochemical cell composition in the shake-flask experiments.

Typically 2 ml of an oil phase was mixed with an equal amount of an aqueous phase containing 5 mM LiTB and 10 mM HCl. The solution mixture was stirred vigorously for a given reaction time, and the phases were separated from each other after the experiment. The oil phase could be analysed by ultramicroelectrode voltammetry or UV-Vis spectroscopy.

3.2.1 Analysis of the H₂O₂ Produced in the Two-Phase Reaction

The aqueous phase could be analysed for hydrogen peroxide by two colorimetric UV-Vis spectroscopy methods, with NaI⁷⁶ or titanium oxalate (TiOx).⁷⁷ Solid NaI was added to 1 mL of the aqueous phase (NaI concentration of 0.1 M) and left to react for 30 minutes in the dark, by which time the hydrogen peroxide present in the sample oxidized iodide to I₃⁻.⁷⁸ The absorbance of triiodide was measured at 352 nm using a Varian Cary 50 Conc spectrophotometer and a quartz cuvette with an optical path length of 0.1 cm. The same setup was used for all UV-Vis measurements. Alternatively, the H₂O₂ content was analysed with titanium oxalate: a 1 mL sample was acidified with sulphuric acid and mixed with a potassium titanium oxalate solution, which reacts with hydrogen peroxide to form a yellow complex. The absorbance was measured at 400 nm⁷⁷ (optical path length of 1 cm). The slight deviations observed between the two methods arise from the fact that the NaI method is more sensitive ($\epsilon = 27600 \text{ M}^{-1} \text{ cm}^{-1}$)⁷⁸ than the TiOx assay ($\epsilon = 935 \text{ M}^{-1} \text{ cm}^{-1}$),⁷⁷ and is therefore more reliable for determining low H₂O₂ concentrations. Moreover, the relative experimental error associated to the latter method is quite larger with respect to the former one, primarily because of the lower absorbance readings and by the large impact of the perturbations induced by the presence of small droplets of immiscible organic solvent in the aqueous test solution. On the other hand, the NaI test can be interfered by other oxidizing species, so the TiOx method should be more specific. The uncertainty for the percentage of hydrogen peroxide production resulting from the inaccurate absorbance readings for the NaI method was estimated as 1% while the value for TiOx method was 8%.¹¹

3.3 Ultramicroelectrode Experiments

Ultramicroelectrode voltammetry was used to measure the redox potentials and diffusion coefficients of the species, as well as the ratio of the oxidized and unreacted electron donors after the shake flask experiments, by measuring cyclic voltammograms (CVs) at a scan rate of 20 mV s^{-1} with a Pt (25 μm diameter), a carbon fibre (10 μm diameter) and a glassy carbon (10 μm diameter) ultramicroelectrodes (UMEs) with a CHI900 electrochemical workstation (CH Instruments, Austin, USA). A three-electrode system with a Pt wire as the counter electrode and a Ag/AgTB wire as the reference electrode (diameter = 0.5 mm, made by electrolysis of a Ag wire in 10 mM LiTB solution) was employed. The potential scale could be calibrated with the addition of decamethylferrocene (0.04 V vs. SHE in DCE⁷⁹ and 0.06 V vs. SHE in DCB^{IV}) at the end of the voltammetry experiments.

Fabrication of the Pt and carbon fibre UMEs was performed as described previously⁸⁰: a 25 μm diameter Pt wire or a 10 μm -diameter carbon fibre was sealed at one end of a glass capillary by a Bunsen burner. Afterwards, the glass capillary with a sealed Pt wire or carbon fibre was subject to a vacuum system for *ca.* 30 min and the capillary was slowly sealed onto Pt wire or the carbon fibre by heating it with a resistor heater coil (David Kopf Instruments, USA). The electrical connection between the Pt wire or carbon fibre and a tin/copper wire was made by melting tin powder inside the capillary.

3.4 Electrospray Ionization Mass Spectrometry

Biphasic electrospray ionization mass spectrometry (ESI-MS) has been used previously to study interfacial complexation at the liquid-liquid interface,⁸¹⁻⁸⁶ but in Publication III the technique was utilised to follow complex biphasic reactions. A dedicated microchip shown in Figure 7 was used as an emitter for ESI-MS to analyse the products from the two-phase reactions. A DCB phase containing 5 mM FcMeOH was brought into contact with an aqueous phase containing 5 mM LiTB and 10 mM HCl either on the microchip shown in Figure 7 or in a shake-flask experiment (see Section 3.2). Samples taken from the oil phase or the fresh solution were infused via channel A at the flow rate of 6 $\mu\text{l/h}$, while channel B was blocked. A sheath flow of ESI buffer (50% water, 49% methanol and 1% acetic acid) was infused via channel C at the flow rate of 54 $\mu\text{l/h}$ to stabilize ESI performance.

For online analysis of the reaction products, the aqueous and oil phases were infused into different channels of the microchip (A and B) at equal flow rates with a syringe pump and the ESI buffer was infused into channel C. The total flow rate of the outlet was kept constant at 60 $\mu\text{l/h}$, while the flow rates in channels A and B were varied for various reaction times. The reaction volume in the microchip is estimated as 2 cm \times 50 μm \times 100 μm , and is located after the joint of channels A and B and before the joint of channels A and C. High voltage (3.7 kV) was applied to the electrode shown in Figure 7 to induce the ESI. A linear ion trap mass spectrometer (Thermo LTQ Velos) was used to characterize the emitted ions.

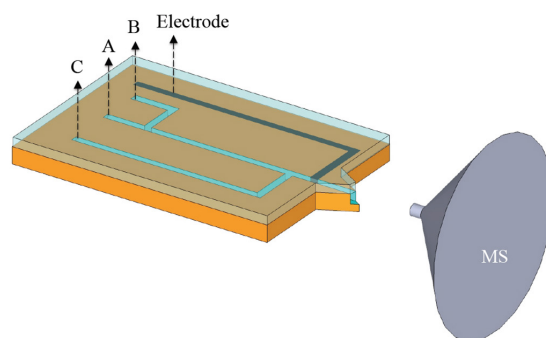


Figure 7. The dedicated microchip for MS characterization of products in the biphasic reactions.^{III}

3.5 Fuel Cell Experiments

A flow fuel cell utilising a liquid-liquid interface shown in Figure 8 was presented in Publication IV. It consists of aluminium endplates (can be thermostated) and graphite flow channel plates (Tanso AB). A polytetrafluoroethylene (PTFE) flow channel for aqueous phase (thickness = 3 mm) was placed between the flow channel plates. On the anode side the flow channel plate was covered by a gas diffusion layer (woven carbon, 60% PTFE, Cadillac Products) and the Pt electrode on carbon support (E-TEK, 0.25 mg Pt/cm²). The aqueous flow was separated from the anode by a Nafion 115 membrane (DuPoint). On the cathode similar gas diffusion electrode is used, covered with a gelled organic phase. The area of the oil-water interface was 4.14 cm². The cell was tightened with eight bolts, with the torque of 5 Nm.

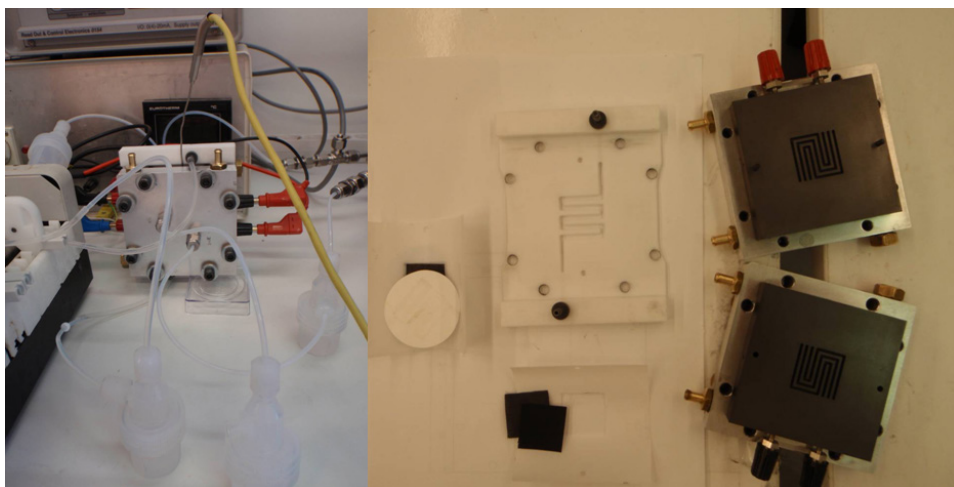


Figure 8. The realization of the flow fuel cell.

The Pt electrodes were cleaned with 1 M methanol for 30 min and washed with Milli-Q water and acetone. Gelled organic phase (gelled by dissolving 50 mg dm^{-3} of polyvinylchloride (PVC) into the DCB phase at $100 \text{ }^\circ\text{C}$) was cast on the Teflon mould on a gas diffusion electrode (E-TEK, 0.25 mg Pt/cm^2). Thickness of the gel layer was controlled with the mould thickness. Fc, DMFc, DcMFC and TTF were used as mediators and 5,10,15,20-meso-tetraphenylporphyrin cobalt (CoTPP) as a catalyst. The supporting electrolyte was 5 mM BATB. About 10 g of 10 mM LiCl + 10 mM HCl solution was weighed into the aqueous circulation tank. The aqueous flow rate was 0.5 ml/min and the flow rates of the gases were 20 ml/min. Chronoamperometric or galvanostatic experiments were performed, and the hydrogen peroxide concentration was determined afterwards from the water circulation by the potassium iodide method.⁸⁷ The efficiency of H_2O_2 production was calculated from the concentration of H_2O_2 in the water circulation, circulated volume and the charge passed during the experiment. Since the polarisation of the anode is negligible due to fast kinetics and mass transport of the electrode reaction, the anode can be regarded as a dynamic hydrogen electrode, a combined reference and counter electrode for fuel cell measurements.⁸⁸

4 Proton-coupled Electron Transfer at Liquid-Liquid Interfaces

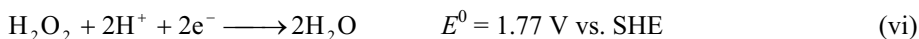
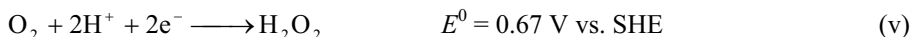
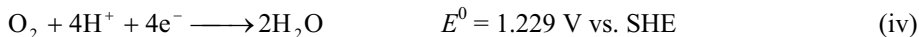
4.1 Proton-coupled Electron Transfer Reactions

Many of the important energy conversion reactions like photosynthesis and cell respiration involve oxidation reduction reactions with both the transfer of electrons and protons. In nature, these steps are coupled, thus avoiding high-energy transition states and increasing the turn-over rate of the reactions. To improve our understanding of the key reactions in respiration, photosynthesis and energy conversion in fuel cells, the proton-coupled electron transfer (PCET) has been the subject of numerous experimental and computational studies.⁸⁹⁻⁹¹ With this understanding, better catalysts could be designed for improved efficiency.

The reduction of protons according to either the Volmer or Heyrovský mechanisms can be considered as one of the simplest PCET reactions.



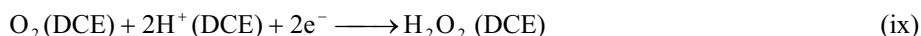
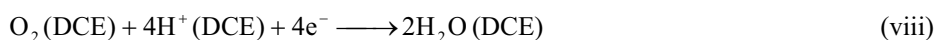
Other important PCET reactions include oxygen reduction and carbon dioxide reduction. Oxygen reduction is a multi-electron transfer process involving a number of steps and intermediates with reduction occurring through a four-electron pathway to produce water (Reaction iv), or a two-electron pathway to produce hydrogen peroxide (Reaction v).⁹² The hydrogen peroxide can also be further reduced to water or decomposed to water and oxygen as shown in Reactions vi and vii.



All of these reactions are of great importance for energy applications and they all can be studied at liquid-liquid interfaces.¹⁰

4.2 Oxygen Reduction at the ITIES

Oxygen reduction is a complex process, and the dominating pathway depends strongly on pH, potential, and catalyst material.⁹² The strength of the O–O bond is very high ($\Delta H = -497 \text{ kJ mol}^{-1}$ ⁶¹), hence breaking this bond requires a very efficient catalyst or a very high overpotential. This high driving force is achieved at liquid-liquid interfaces with the use of suitable electron donors in the oil phase: if protons from the DCE phase are used for oxygen reduction instead of aqueous protons, the standard potentials for Reaction viii and ix are $E^0 = 1.749 \text{ V}$ and 1.166 V vs. aqueous SHE⁶⁸ as shown in Figure 3.



This difference arises from the increased reactivity of protons in the oil phase, as they are less stabilised by the organic solvent. Nonetheless, the energy cost of transferring the protons into the DCE is 53 kJ mol^{-1} or equivalent of the Galvani potential difference of 0.55 V .⁶⁹ As a result, for non-catalysed oxygen reduction to take place at ITIES, protons are needed to be transferred from the aqueous phase to the oil phase in the presence of an electron donor of moderately high reducing ability in order to activate the O–O bond.

Cunnane *et al.* were the first to show by voltammetry that oxygen could be reduced by DcMFC.⁹³ Following this, Kihara *et al.* showed that tetrachlorohydroquinone in oil phase could reduce oxygen to water or hydrogen peroxide, depending on the potential difference applied at the w-DCE,⁹⁴ whilst Liljeroth *et al.* demonstrated that electrogenerated fullerene anions could also reduce oxygen at ITIES.⁹⁵ These works are some of the earliest studies of a PCET reaction at the ITIES, describing a system where the reduction of oxygen in DCE requires a suitable electron donor in the oil phase and a proton source in the aqueous phase. In more recent years, the oxygen reduction at the ITIES by direct electron donors such as different ferrocene derivatives (for example DcMFC, DMFc and Fc^{78,96}) or TTF⁹⁷ has become a subject of a renewed interest. The rate of the uncatalysed reaction is directly depended on the driving force (*i.e.* redox potential) of the electron donor.⁹⁸ The reactions with DMFc, Fc and TTF are rather slow, but the reaction rates can be enhanced significantly by various molecular or colloidal catalysts, as described in Chapter 5. In contrast, hydrogen peroxide was produced with ferrocene derivatives, whilst four-electron reduction to water was achieved with TTF.⁹⁷

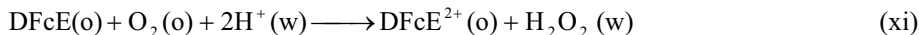
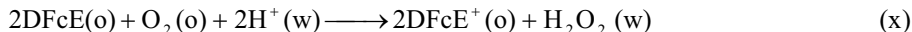
A key finding was that the interfacial Galvani potential difference could be used to drive protons from the aqueous to the oil phase, thus enabling a high enough driving force to overcome the kinetic limitations for reduction of oxygen to hydrogen peroxide by DcMfc.⁷⁸ Additionally, in the absence of oxygen, even hydrogen evolution by DcMfc has been shown to occur.⁹⁹ Su *et al.* also demonstrated that the oxygen reduction reaction could be performed in the shake flask experiments, driven by the distribution of HTB between the two phases.⁷⁸ The oxidation of the electron donor could be followed by UV-Vis with hydrogen peroxide production confirmed both by treating the aqueous phase with NaI, and also by scanning electrochemical microscopy (SECM) measurements on the aqueous side of the interface.⁹⁶

Oxygen reduction by metallocenes at a liquid/liquid interface has been proposed to proceed in two steps: proton transfer from the aqueous to the oil phase facilitated by the metallocene followed by homogenous oxygen reduction in the oil phase. In the case of DcMfc formation of the hydride DcMfcH⁺ with proton binding to the iron is the first step.¹⁰⁰ Density functional theory (DFT) calculations suggest that instead of the coordination of a triplet molecular oxygen to the iron atom (spin-forbidden)¹⁰¹ or insertion into Fe–H bond, the reaction with oxygen proceeds through a delocalized triplet transition state, leading to the formation of DcMfc⁺ and a hydrogen peroxy radical.¹⁰⁰ In addition, a mechanism where molecular oxygen is coordinated between two protonated ferrocenes has been proposed.¹⁰² This mechanism has some similarities with the oxygen reduction by cofacial metal porphyrins,^{103,104} mimicking the oxygen reduction occurring in the bimetallic iron/copper centre of CcO.¹²

4.2.1 Oxygen and Hydrogen Peroxide Reduction by 1,2-diferrocenylethane

In Publication I oxygen reduction by 1,2-diferrocenylethane (DFcE), a multi-ferrocenyl compound, was studied at the polarised w-DCE interface. This compound has been successfully used as an electron donor for electron transfer studies at the liquid-liquid interface,^{105,106} and previous NMR results indicate that protonation of both ferrocenyl groups should take place in boron trifluoride monohydrate solution.¹⁰⁷ Formation of the dihydride DFcEH₂²⁺ should enable the oxygen reduction to hydrogen peroxide with molecular oxygen sandwiched between the protonated iron centres, using only one DFcE molecule. Oxygen reduction by DFcE can be described by Reactions x or xi. Ferrocene derivatives also catalyse

decomposition and also further reduce hydrogen peroxide, according to Reactions xii and xiii.¹



Cyclic voltammetry of DFcE on a carbon fibre UME confirmed that DFcE has two oxidation waves corresponding to $\text{DFcE}^+/\text{DFcE}$ and $\text{DFcE}^{2+}/\text{DFcE}^+$ in DCE with the half-wave potentials $E_{1/2}$ at 0.565 V and 0.770 V vs. SHE, and hence the reduction of oxygen by both DFcE and DFcE^+ is thermodynamically feasible.¹ The CVs obtained with the four-electrode electrochemical cell in the presence and absence of DFcE is shown in Figure 9.

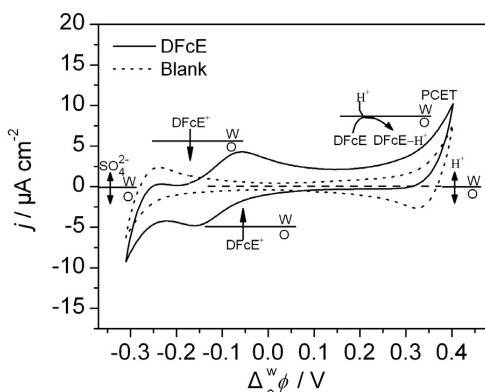


Figure 9. Cyclic voltammograms obtained with 50 mM H_2SO_4 + 10 mM Li_2SO_4 in the aqueous phase and 5 mM BATB in DCE in the absence of DFcE (dotted line) and in the presence of 5 mM DFcE (solid line) in the DCE phase; scan rate 50 mV s^{-1} .¹

A potential window from about -0.30 to 0.40 V in the Galvani potential scale can be obtained with the supporting electrolytes $\text{H}_2\text{SO}_4/\text{Li}_2\text{SO}_4$ and BATB in aqueous and DCE phases, respectively. The potential window is limited by the reversible transfer of H^+ and SO_4^{2-} from water to DCE at positive and negative potentials, respectively. The current increased remarkably on the positive limit of the potential window upon addition of 5 mM DFcE, and no clear return peak was observed for the transferred protons (solid line in Figure 9), indicating that protons were consumed in a homogeneous reaction according to Reactions x or xi. The transfer of DFcE^+ generated in the oxygen reduction is observed in the range of -0.2

to -0.05 V with the half-wave potential at -0.12 V and the onset potential of the proton transfer took place at lower potentials than in the absence of DFcE. This indicates that DFcE can facilitate the proton transfer as suggested earlier in the case of DcMfc.⁷⁸ A hysteresis observed in Figure 9 after reversal of the scan direction at around 0.4 V shows that oxygen reduction is not fast enough to consume all the transferred protons in the time scale of the experiment. Similar results have been reported previously by Su *et al.* when DMFc was used as electron donor for the oxygen reduction at the ITIES.⁷⁸ The forward current enhancement by DFcE is less than that by DMFc, indicating slower kinetics due to the difference in electrochemical driving force (0.04 V for DMFc vs. 0.57 V for DFcE vs. aqueous SHE). No sign of DFcE²⁺ formation could be observed.

A fresh solution of DFcE in DCE has a brown colour and displays an absorption band in the UV-Vis spectrum at 436 nm (dotted curve in Figure 10A).¹ After the two-phase shake flask reaction (reaction time = 10 min) the DCE phase turned dark green, and a broad absorption band at $\lambda_{\text{max}} = 619$ nm (dash-dotted curve in Figure 10A) corresponding to DFcE⁺ appeared.¹ The presence of H₂O₂ in the aqueous solution after the shake-flask reaction was confirmed using the NaI method, as represented by the appearance of the I₃⁻ characteristic absorption band at 352 nm (solid curve in Figure 10A). No I₃⁻ signal was observed in the UV-Vis spectrum for the aqueous phase prior to the biphasic reaction.

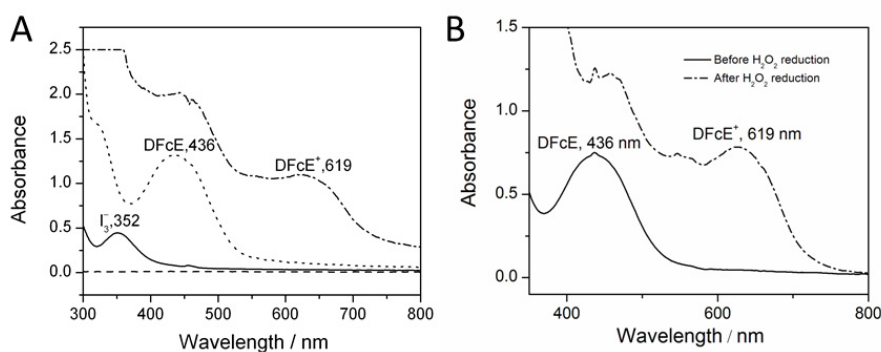


Figure 10. A) UV-Vis spectra of the aqueous phase before (control, dashed line) and after (target, solid line) 10 min of aerobic two-phase reaction under stirring conditions. The dotted and dash-dotted traces correspond to the UV-Vis spectra of DFcE solutions in DCE before and after 10 min of aerobic two-phase reaction under stirring conditions (diluted by half), respectively. For the two-phase reaction: the aqueous phase contained 50 mM H₂SO₄ + 5 mM LiTB (2 mL); the DCE phase contained 5 mM DFcE + 5 mM BATB (2 mL). B) UV-Vis spectra of 2.6 mM DFcE + 5 mM BATB in DCE before (solid line) and after (dashed-dot line) 30 min biphasic hydrogen peroxide reduction inside a glove box (aqueous phase 1 mM H₂O₂ + 10 mM HCl + 5 mM LiTB).¹

The progress of the reaction could also be followed by utilising UME voltammetry. Shake flask experiments with LiTB:DFcE molar ratio of 4 showed that a DFcE conversion of *ca.* 50 % to DFcE⁺ was reached after 1 h of reaction, and this reaction was followed by slow oxidation of DFcE⁺ to DFcE²⁺. After 18 h of reaction about half of the DFcE had been oxidized to DFcE²⁺ and the reaction was completed only after 26 h.¹ The rate of oxygen reduction by DFcE is very slow and the produced DFcE⁺ is also able to reduce oxygen, although at even slower rate, as expected from the higher redox potential. Only small amounts of hydrogen peroxide were detected in the shake flask experiments.

Control experiments for hydrogen peroxide decomposition and reduction (1 mM H₂O₂ in aqueous phase) showed that DFcE can both partition into the aqueous phase to be oxidized by H₂O₂, and also catalyse hydrogen peroxide decomposition. If the Galvani potential difference was controlled by addition of LiTB under a nitrogen atmosphere in a glove box, UV-Vis spectra of the oil phase shows that significant amount of DFcE was oxidized to DFcE⁺ during a 30 min reaction (Figure 10B). Further characterisation was performed with the UME voltammetry showing that reduction of hydrogen peroxide was actually faster than oxygen reduction. This explains why such small amounts of hydrogen peroxide are detected in the shake flask experiments, as oxygen is firstly reduced to hydrogen peroxide, then followed by the faster hydrogen peroxide reduction step.¹

The 0.1 mM DFcE²⁺ DCE solution prepared by 26 h biphasic reaction was studied in a four electrode cell and the comparison of CVs of DFcE and DFcE²⁺ solutions are show in Figure 11. The peaks for the reversible transfer of DFcE⁺ (formed after PCET, where the initial species in DCE is DFcE) and DFcE²⁺ across the w-DCE interface are observed at -0.16 V and 0.00 V, respectively.¹

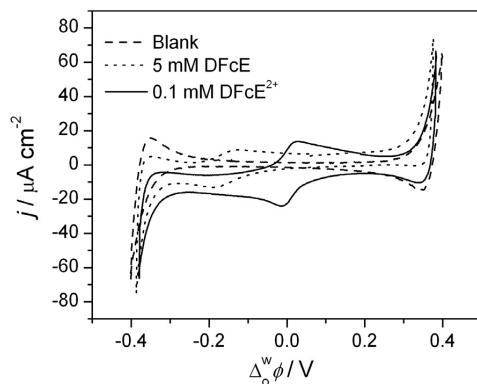


Figure 11. Comparison of iR compensated voltammograms of 5 mM DFcE (dotted line) and 0.1 mM DFcE²⁺ (solid line) solutions in the electrochemical cell with 50 mM H₂SO₄ in the aqueous phase and 5 mM BATB in DCE. For comparison, blank CV recorded with iR compensation is also included. Scan rate: 50 mV s⁻¹.

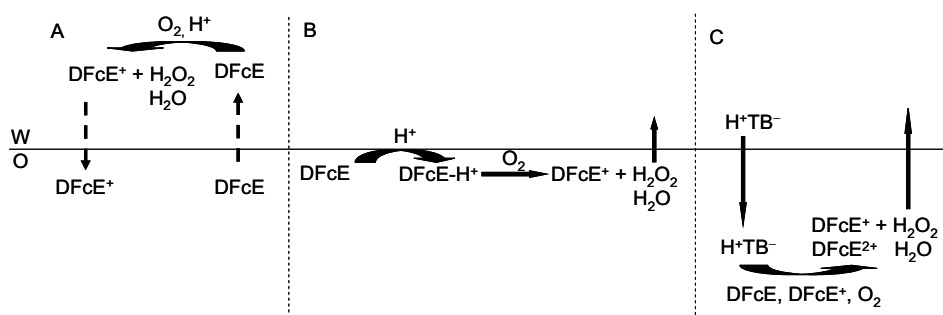
DFcE⁺ was formed according to Reactions x or xiii, as described earlier. The peak separation of the transfer peak of DFcE²⁺ was about 30 mV, confirming that the transferred species had a charge equal to 2.¹ These measurements indicate that oxygen reduction by DFcE does not proceed through an oxygen molecule sandwiched inside the two protonated iron centres of DFcE, as hypothesized by Fomin,¹⁰² as no DFcE²⁺ is observed in the four-electrode cell measurements. Thus it is more likely that the reaction proceeds in a similar way as proposed by Girault *et al.* for DcMfc through a delocalized triplet transition state, leading to the formation of DFcE⁺ and a hydrogen peroxy radical.¹⁰⁰ This hydrogen peroxy radical will then undergo a fast reaction with DFcE and H⁺ to form H₂O₂. Alternatively, the reaction could still proceed through molecular oxygen located between two DFcE–H⁺ molecules, but this would require a trimolecular reaction deeming it more unlikely. Another interesting question is whether the electron is donated by the protonated iron or the non-protonated one. In this case, the protonation will probably take place outside of the molecule due to the steric hindrance of the other ferrocenyl group, and thus the non-protonated iron would be too far away to have an effect on the reaction.

Hydrogen peroxide reduction by ferrocene derivatives has been briefly mentioned previously in the literature in order to explain observed four-electron reduction of molecular oxygen but it has been less well studied.^{101,108} A mechanism for ferrocene oxidation by hydrogen peroxide suggested by Fomin indicates that the protonated ferrocene can react with H₂O₂ to form water, Fc⁺ and OH· radical, which further reacts with Fc and a proton to produce water.¹⁰² From this point of view, DFcE seems ideal for hydrogen peroxide reduction, as

hydrogen peroxide can react with the protonated ferrocenyl group and the generated OH· radical can then easily oxidize the other ferrocenyl group.

Taking into account all the previous results, it can be proposed that O₂ reduction by DFcE can take place at the w-DCE interface or in the bulk DCE phase (see Scheme 3B). The first step consists of the protonation of DFcE to form the DFcE-H⁺ in DCE phase, as observed with other metallocenes. Then, the formed DFcE-H⁺ is attacked by dissolved O₂ in DCE side at the w-DCE interface or in the DCE bulk to produce H₂O₂ or water and DFcE⁺.¹ Hydrogen peroxide reduction is assumed to proceed in a similar manner, but the reaction is expected to take place close to the interface due to the low solubility of H₂O₂ in DCE.

DFcE can also partition into the aqueous phase and react with aqueous oxygen or hydrogen peroxide (see Scheme 3A), as shown by H₂O₂ decomposition experiments. In that case no protons were present in DCE, so the observed DFcE⁺ in the aqueous phase was the reaction product of H₂O₂ reduction by partitioned DFcE.¹ In biphasic shake-flask experiments, the protons are extracted to the oil phase by TB⁻. This fast extraction is followed by slower oxygen reduction initially by DFcE and later by DFcE⁺ in the bulk DCE phase, as outlined in Scheme 3C. From voltammetry and shake-flask results, it can be concluded that the reaction is controlled by the Galvani potential difference applied at the ITIES, which mainly functions as the driving force for the proton pump at the soft molecular interface.¹



Scheme 3. Proposed mechanism of O₂ reduction by DFcE at the W/O interface. W = aqueous phase, O = DCE phase. Hydrogen peroxide can replace oxygen in the scheme, producing water. (A): DFcE partitions to aqueous phase and reacts with protons and oxygen or hydrogen peroxide to produce H₂O₂ or H₂O. (B): Protons facilitated transfer into DCE phase by DFcE followed by oxygen or hydrogen peroxide reduction to H₂O₂ or H₂O partitioning back to aqueous phase; (C): Biphasic shake-flask reaction where TB⁻ extracts protons to DCE phase, followed by oxygen and hydrogen peroxide reduction in the bulk of DCE phase.¹

5 Electrocatalysis at the ITIES

Catalysis is by definition a process where addition of a catalyst reduces the activation energy of the reaction, and the catalyst is not consumed in the reaction. In electrocatalysis, the same thing occurs in an electrochemical reaction: for example, addition of Pt nanoparticles on a carbon electrode significantly decreases the overpotential of hydrogen evolution. The activation energy can, in this case, be described by the activation overpotential as the reactions are driven by electrode potential. In addition, electrocatalysts can be designed to favour certain reaction pathways. Generally, electrocatalysis is usually considered only on a solid electrode surface, but another type of interface where electrocatalysis can be utilised is the interface between two immiscible electrolytes, and this chapter concentrates on this topic. The types of electrocatalysts can be divided between colloidal catalysis, where a solid particle adsorbed at ITIES acts as a catalysts and molecular catalysis, where reactions are catalysed by molecules, usually adsorbed at the ITIES.

5.1 Colloidal Electrocatalysis at the ITIES

ITIES can be functionalized by nanoparticles in two ways: heterogeneous *in situ* electrochemical generation of metal nanoparticles, or by adsorption of chemically prepared particles on the interface. Generally, the minimization of the energy favours the adsorption of particles on the interface (depending on the surface tension between different phases in the system). The utilisation of colloidal catalysts was first reported by Schiffrin and Cheng: *in situ* generated Pd nanoparticles were shown to catalyse dehalogenation of 2-bromoacetophenone at the w-DCE interface.¹⁰⁹ Kontturi *et al.* showed that the same reaction could be performed with *ex situ* generated Au or Pd particles, with DcMFC as an electron donor, when the Galvani potential difference was controlled with a distribution of a common ion.¹¹⁰ It was also suggested that the colloidal catalysts could behave as bipolar electrodes, with the oxidation taking place in one phase and reduction in another.¹¹¹

Later, a similar approach has been used to perform oxygen reduction by DcMFC, catalysed by *in situ* generated Pt or Pd nanoparticles adsorbed at w-DCE interface.¹¹² If the same reaction was performed in anaerobic conditions, Pt and Pd nanoparticles could catalyse hydrogen evolution.⁷⁹ Colloidal Pd particles, generated *in situ* from PdCl_4^{2-} by Fc were also shown to catalyse photoinduced electron transfer between tetracyanoquinodimethane in DCE and

photoexcited zinc tetrakis(carboxyphenyl)-porphyrin in the aqueous phase.¹¹³ More recently, it was demonstrated that also MoS₂ particles adsorbed at ITIES are effective hydrogen evolution catalysts.¹¹⁴ DFT calculations by Nørskov *et al.* have shown that the edge sites of MoS₂ are the most active sites for H₂ evolution, having Gibbs energy of adsorption for hydrogen close to zero.¹¹⁵

A method to measure the rate constants of hydrogen evolution reaction with different colloidal catalysts adsorbed at the w-DCE interface was demonstrated by Ge *et al.*¹¹⁶ The Galvani potential difference was adjusted with the addition of LiTB into the aqueous phase: with hydrophobic TB⁻ transferred into the DCE phase with equal amount of protons to maintain electroneutrality. Consequently, protons could be reduced by DcMFC in the DCE phase. The progress of the reaction can be easily followed with UV-Vis, by measuring the absorption of DcMFC⁺ at 779 nm and the validity of the method was confirmed by analysing the amount of generated hydrogen by gas chromatography.¹¹⁴ The relative abilities of nanocrystalline MoS₂, exfoliated MoS₂, and MoS₂ nanoparticles grown on either graphene or mesoporous carbon particles were investigated as hydrogen evolution catalysts by the UV-Vis method. The results showed that conductive carbon support increased the reaction rate by the factor of 3 to 12 by two ways. Firstly the support facilitates the formation of small and highly dispersed MoS₂ nanoparticles with increased abundance of catalytic edge sites in comparison to MoS₂ synthesised in solution.^{117,118} Secondly, the catalyst support increases the cross-section of reaction area between DcMFC and the catalyst, as now electrons can be injected anywhere on the conductive carbon support to be used by the protons adsorbing at the catalytic MoS₂ edge sites, and thus no direct injection of an electron into the catalyst is needed. The enhanced rate observed for MoS₂ on mesoporous carbon particles in comparison to its graphene analogue indicates that the large surface area of mesoporous carbon allows for better loadings of small, highly dispersed MoS₂ centres than what is possible on the surface of comparatively flat graphene.¹¹⁶

5.2 Molecular Electrocatalysis at the ITIES

The studies of molecular electrocatalysis at ITIES date back to the pioneering work by Volkov *et al.* since the 1970s,¹¹⁹ as summarized in reviews by Volkov in 1998^{120,121} and more recently by Su *et al.*¹²² Their work is based on the fact that a change in the Galvani potential induces a change in the surface potential of the oil-air interface and this could be measured

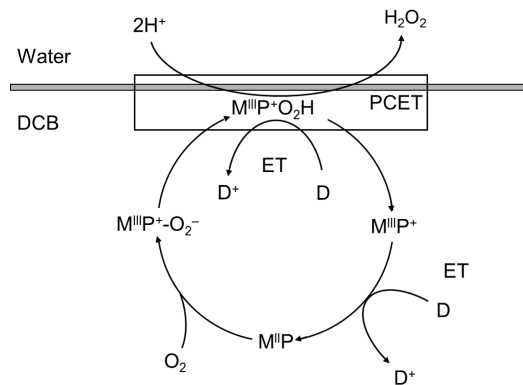
with a Kelvin probe. This elegant technique measures the changes in the surface potential of the oil phase with a vibrating gold electrode and Volkov *et al.* used this technique to study redox reactions at water-alkane interfaces. They reported that molecular catalysts like chlorophylls or porphyrins could catalyse proton-coupled electron transfer reactions between lipophilic electron acceptors like 2*N*-methylamino-1,4-naphthoquinone or vitamin K₃ dissolved in octane and hydrophilic electron donors (for example nicotinamide adenine dinucleotide (NADH) or potassium ascorbate) in the aqueous phase,¹²¹ and they also demonstrated the reduction of molecular oxygen by NADH.¹²³ All of these reactions can be considered as proton-coupled electron transfer reactions, where a proton is transferred from aqueous phase into the oil phase. Volkov *et al.* also used the same Kelvin probe technique to demonstrate that enzyme complexes like CcO, succinate-cytochrome *c* reductase and NADH-CoQ reductase catalyse charge transfer across the liquid-liquid interface.¹²⁰

Another example of enzyme catalysed reactions was given when Williams *et al.* demonstrated glucose oxidase catalysed oxidation of β-D-glucose by DMFc⁺ cations electrogenerated at a SECM tip in DCE, while the Galvani potential difference across the interface was controlled by the distribution of a common ion.¹²⁴ Osakai *et al.* employed cyclic voltammetry with a four-electrode cell to show that this reaction is not in fact heterogeneous but takes place homogeneously in the aqueous phase by ion transfer mechanism: DMFc⁺ cations transfer into the aqueous phase to be reduced by glucose (catalysed by glucose oxidase). Generated DMFc partitions into the oil phase, so no back transfer of DMFc⁺ is observed in the experiments.¹²⁵

Electrocatalysis of oxygen reduction is one of the most studied topics in electrocatalysis at ITIES. As described in Section 4.2, this PCET reaction requires an electron donor in the oil phase and a source of protons in the aqueous phase. There are two ways to catalyse oxygen reduction at the ITIES. First, since the reaction takes place when protons are present in the oil phase, it is evident that the reaction can be catalysed by addition of hydrophobic bases like different aniline derivatives to facilitate the proton transfer.^{126,127} The efficiency of the catalysts depends on their basicity (affinity for protons).¹²⁷ The second way is to use catalysts that weaken the O–O bond by coordinating to the molecular oxygen. One way to do this is to utilise different N₄-macrocyclic metal complexes. This group of molecules has been known to catalyse oxygen reduction since the first report by Jasinski in 1964 described the activity of cobalt phthalocyanine (CoPc) as an oxygen reduction catalyst.¹²⁸ Recently it was also shown that CoPc acts as a molecular catalyst for oxygen reduction at ITIES,¹²⁹ and the catalytic effect could be improved by using fluorinated CoPc.¹³⁰ The different N₄-macrocyclic

complexes investigated as oxygen reduction catalysts have been reviewed in detail in a recent Licentiate's thesis.¹³¹

Samec *et al.* showed that well-known molecular catalyst 5,10,15,20-meso-tetraphenylporphyrin cobalt (CoTPP) could catalyse oxygen reduction at ITIES by DcMfc.¹³² Partovi-Nia *et al.* showed that electron donors of lesser driving force (like DMFc and Fc) could also be used to perform the reaction.¹³³ The catalytic cycle shown in Scheme 4 for these systems was found to be similar to the cycle proposed by Fukuzumi *et al.* for homogeneous reactions, where the proton source was perchloric acid.^{134,135} Also oxygen reduction by phthalocyanines has been suggested to follow the same mechanism.¹²⁹ Metalloporphyrin ($M^{II}P$) forms a complex with oxygen and takes two protons from the aqueous phase and an electron from an electron donor in a PCET step, releasing hydrogen peroxide. The catalyst is oxidized to $M^{III}P^+$ in the process, and can be reduced by the electron donor, completing the catalytic cycle.



Scheme 4. Reaction scheme for oxygen reduction by a mediator catalysed by metal porphyrins.¹¹ ET stands for electron transfer and PCET is proton-coupled electron transfer. Adapted from Ref. 133.

Typical example of the oxygen reduction catalysed by CoTPP observed in with cyclic voltammetry at w-DCB interface is shown in Figure 12.

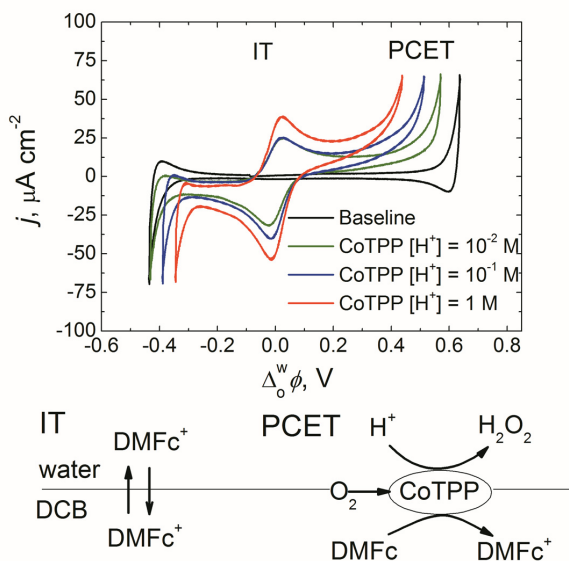


Figure 12. Cyclic voltammograms of 1 mM CoTPP with 5 mM DMFc in 1,2-dichlorobenzene (DCB) for various proton concentrations in the aqueous phase. The baseline corresponds to the CV of the oil phase with the supporting electrolyte in contact with 10 mM HCl. Mechanisms of ion transfer (IT) and proton coupled electron transfer (PCET) are described below.¹¹

The voltammogram shows a reversible ion transfer wave of the oxidized mediator, DMFc^+ , at -0.02 V, proving that DMFc is oxidized by oxygen in the presence of CoTPP. Reversible chloride transfer takes place at the negative end of the window and an irreversible current wave can be attributed to a PCET reaction at the positive limit of the window, producing hydrogen peroxide or water. The limits of the potential window shift towards the middle of the window as the HCl concentration is increased (shift of *ca.* 60 mV per $\log c_{\text{HCl}}$) as described by Equation 2.

Different molecular catalysts such as cobalt(II) octaethylporphyrin (CoOEP),¹³⁶ cobalt(II) porphine (CoP),⁶⁸ and amphiphilic cobalt(II) 2,8,13,17-tetraethyl-3,7,12,18-tetramethyl-5-p-amino-phenylporphyrin (CoAP)¹³⁷ and fluorinated amphiphilic free-base porphyrin (H_2FAP)¹³⁸ have been shown to catalyse oxygen reduction at the liquid-liquid interface. Introduction of amphiphilic groups to porphyrin enhanced the adsorption of the catalyst to the ITIES, showing improved catalytic activity over unsubstituted analogue CoOEP.¹³⁷ Interestingly, also free-base porphyrins were found to be active towards oxygen reduction, mostly due to their ability to facilitate the proton transfer but also because of the ability of the protonated porphyrin to coordinate molecular oxygen with the reaction product being mostly hydrogen peroxide.^{139,140} However, the catalytic cycle was found to be inhibited by water and

by the counter anion in a homogeneous reaction, and this is likely to be the case also with the metalloporphyrins.^{141,142} Recently, also self-assembled molecular “rafts” of the oppositely charged water-soluble porphyrins, cobalt tetramethylpyridinium porphyrin and cobalt tetrasulphonatophenyl porphyrin, were shown to be excellent catalysts for the interfacial four-electron reduction of oxygen, when TTF was used as an electron donor. The catalytic activity and selectivity of the self-assembled catalyst toward the four-electron pathway was described to be as good as that of the “Pacman” type cofacial cobalt porphyrins.¹⁴³

The examples above show that voltammetry at liquid-liquid interfaces is an efficient tool to study and compare molecular electrocatalysts. The role of the molecular catalyst is to bind molecular oxygen to activate the oxygen reduction and it should have a high affinity for protons (observed as facilitated proton transfer) and electrons (observed as irreversible proton transfer). Since hydrogen peroxide and water are extracted to the aqueous phase, ITIES allows the combination of solvent extraction with electrocatalysis.

In Publication IV, it was shown with the four-electrode cell and biphasic measurements that all the four different redox mediators studied (Fc, DMFc, DcMFC and TTF) could be utilised as electron donors for oxygen reduction catalysed by CoTPP also in DCB (Figure 13). The presence of the catalyst greatly enhanced the reaction rate, and the reaction mechanism was the same as outlined earlier for oxygen reduction in DCE (Scheme 4).

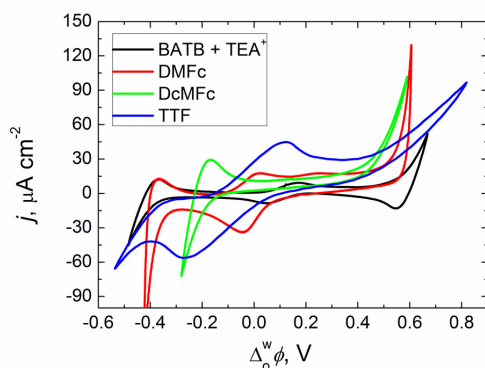


Figure 13. CVs in the presence of only the supporting electrolyte (solid black) and the effect of the different mediators (5 mM) in the presence of 1 mM CoTPP in DCB.^{IV}

Figure 13 shows that a clear PCET wave is observed for each mediator at the positive end of the potential window also in DCB. The negative ends of the window are limited by the transfer of Cl^- or by transfer of DcMFC^+ (solid green curve in Figure 13).

5.2.1 Biomimetic Catalysis for Oxygen Reduction with Cofacial Porphyrins

The development of an effective, selective and cheap catalyst for oxygen reduction is of significant importance for many applications. In nature, oxygen reduction is used in aerobic energy conversion, so can we mimic nature to develop better catalysts. Oxygen reduction is catalysed by a bimetallic active centre of CcO bound in the lipid bilayer of the cell membrane (Figure 14).¹² The active centre of CcO consists of a bimetallic iron porphyrin/copper heterodinuclear centre, where a copper atom coordinated by three histidines is located above the iron centre of the heme.^{12,13}

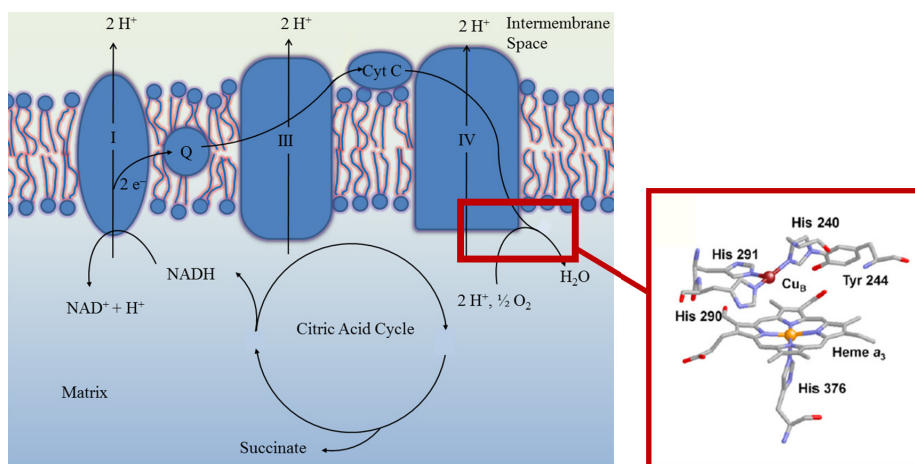


Figure 14. Scheme of the processes related to oxygen reduction catalysed by CcO in mitochondrial membrane, and the active centre of CcO (Structure of the active centre of the CcO adapted with permission from Ref. 13. Copyright 2004 American Chemical Society).

Molecular catalysts with similar active sites can be synthesized and studied as possible oxygen reduction catalysts, which also provides insight into the working of the enzymes.^{144,145} For these reasons different cofacial bimetallic porphyrins sharing a structural similarity with CcO have been synthesized.^{103,104,146} The ability of the cofacial porphyrins to form μ -peroxo complexes of oxygen sandwiched between the two metal atoms (O_2^{2-} like oxygen covalently binding on the both metal atoms) is the key ability to catalyse the breakage of the O–O bond. In Publication II the behaviour of three different cofacial porphyrins (bis(cobalt)porphyrins of 4,5-bis[5-(2,8,13,17-tetraethyl-3,7,12,18-tetramethyl-porphyrinyl)]-9,9-dimethyl-xanthene $Co_2(DPX)$, 2,2-bis[5-(2,8,13,17-tetraethyl-3,7,12,18-tetramethylporphyrinyl)] diphenyl ether $Co_2(DPOx)$, and 4,6-bis[5-(2,8,13,17-tetraethyl-3,7,12,18-tetramethyl-porphyrinyl)] dibenzofuran $Co_2(DPO)$) shown in Figure 15 as electrocatalysts for oxygen reduction at ITIES was studied. Earlier studies with the chosen porphyrins showed high selectivity for

four-electron reduction when adsorbed on a graphite electrode,¹⁰³ or as a homogeneous solution in benzonitrile.¹⁴⁷ In this case different ferrocene derivatives were used as electron donors and HClO₄ was used as a proton source.¹⁴⁷ In homogeneous conditions Co₂(DPX) produces water with 100% efficiency,¹⁴⁷ but when adsorbed on carbon, the selectivity decreases to 72%.¹⁴⁸

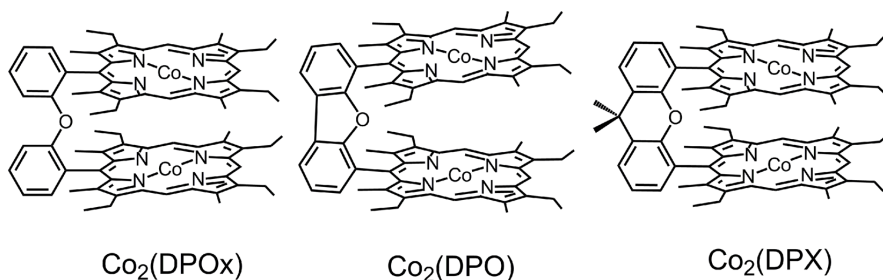


Figure 15. Cofacial biscobalt porphyrins studied in Publication II.

The catalytic activity of the three cofacial biscobalt porphyrins, shown in Figure 15, for oxygen reduction was studied at the liquid-liquid interface with four-electrode cell voltammetry and in shake flask experiments. Voltammetry at the ITIES could be used to compare the affinity of the catalyst-oxygen complex for the protons and shake flask experiments were done to evaluate the selectivity of the catalysts for four-electron reduction of molecular oxygen.^{II} Two different mediators of similar redox potential, DMFc and TTF (Figure 6), were used as TTF has been shown to be unreactive in the presence of H₂O₂⁹⁷ and it is known that ferrocene derivatives catalyse decomposition of hydrogen peroxide.^I Redox potentials of both TTF/TTF⁺ and TTF⁺/TTF²⁺ couples were determined as 0.58 and 1.60 V vs. SHE in DCB with UME voltammetry^{II}, respectively (0.56 V vs. SHE in DCE⁹⁷), and the value for DMFc is 0.57 V vs. SHE^{IV}, so that the thermodynamic driving force for oxygen reduction is almost the same with both mediators.

Figure 16 shows the cyclic voltammograms of 100 μM of the catalysts with 5 mM DMFc. All studied cofacial porphyrins exhibit high catalytic activity towards oxygen reduction as indicated by the large amount of DMFc⁺ formed and by the very small hysteresis observed on the reverse scan at the positive end of the potential window.^{II} The amount of catalyst is far less than that of CoTPP, while obtained current densities are considerably higher (see Figure 12). No catalytic activity was observed in the absence of a redox mediator.

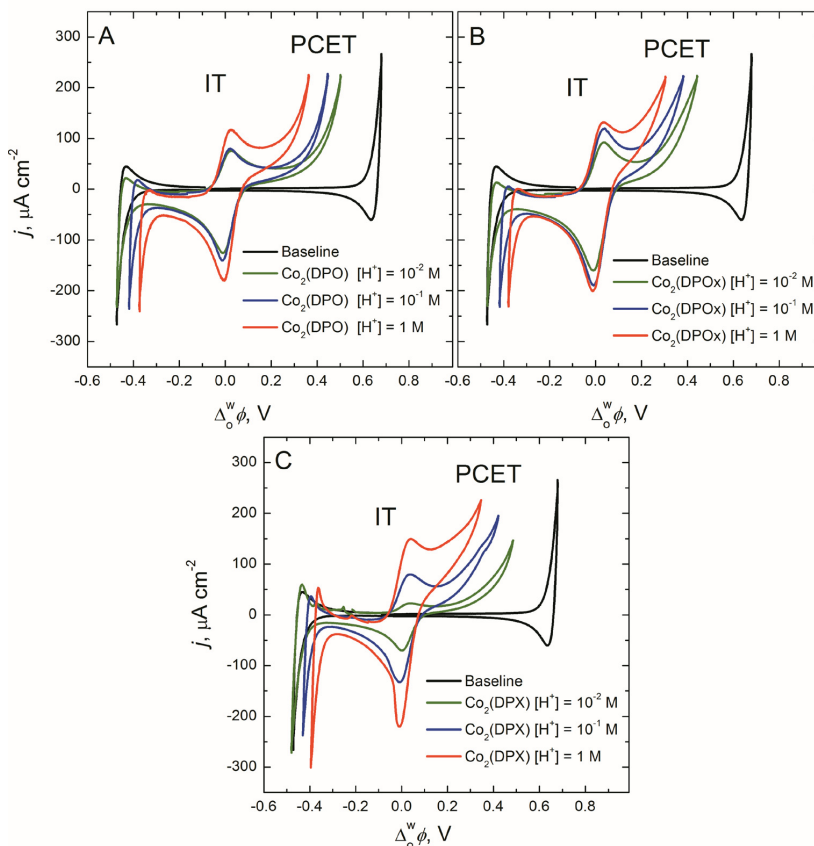


Figure 16. Cyclic voltammograms of 100 μM $\text{Co}_2(\text{DPO})$ (A), $\text{Co}_2(\text{DPOx})$ (B) and $\text{Co}_2(\text{DPX})$ (C) with 5 mM DMFc and 5 mM BATB in DCB for various proton concentrations in the aqueous phase. The baseline corresponds to the CV of 5 mM BATB in DCB in contact with 10 mM aqueous HCl.^{II}

The voltammetry at ITIES gives information about the proton affinity of the porphyrin-oxygen complex: the higher the affinity, the lower the onset potential of the PCET wave as described by Equation 16. Hence $\text{Co}_2(\text{DPOx})$ shows the highest affinity for protons, showing the PCET wave at 0.4 V in pH 2. In comparison, CoTPP shows a PCET wave at 0.55 V in pH 2 and the unfacilitated transfer of protons takes place at 0.6 V, confirming that the cofacial porphyrins have higher affinity for protons than CoTPP.^{II}

The selectivity of different catalysts towards four-electron reduction of molecular oxygen was studied in biphasic reactions, where the Galvani potential difference was determined by the partitioning of a common ion, TB^- as described in Section 3.2. Protons were extracted to the interface and into the oil phase where they reacted with the electron donor in the presence of the catalyst. The conversion of the donor was determined from UME voltammetry and the hydrogen peroxide was assayed with two different colorimetric methods, as described in the

experimental section. Figure 17 shows the UV-Vis spectra of the oil phase before and after the reaction, for a contact time of 30 s. The inset shows the UME voltammograms (vs. DMFc/DMFc⁺) recorded before and after the reaction to determine the amount of mediator consumed during the reaction catalysed by Co₂(DPX).

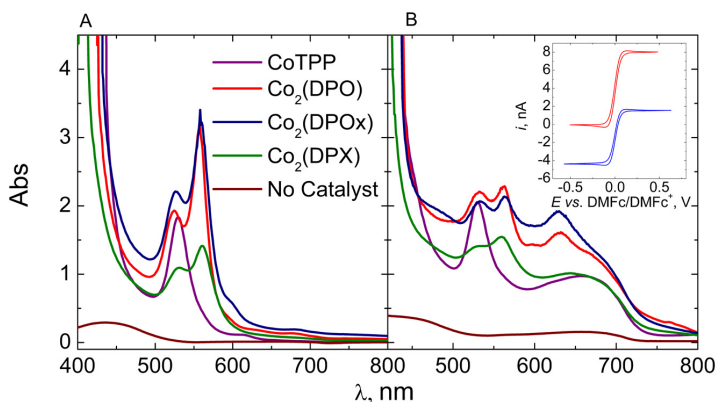


Figure 17. UV-Vis spectra of DCB phases containing 100 μM of catalyst, 2 mM DMFc and 5 mM BATB before (A) and after (B) two-phase reactions. The inset shows the measured UME voltammograms (vs. DMFc/DMFc⁺) before and after two-phase reaction, using 100 μM Co₂(DPX) as a catalyst. The reaction time was 30 s, followed by a 30 s settling time.^{II}

The spectra show that all the porphyrins have strong Q-band adsorption at around 550 nm. DMFc has an absorbance peak at 439 nm and DMFc⁺ has a broad peak at 550–725 nm, the spectral features appearing above 600 nm in Figure 17B demonstrate that DMFc is oxidized during the experiments. Changes in the Q-band absorption of the catalysts relate to the protonation and oxidation of the catalyst.^{II} The results also show that UME voltammetry can be used to monitor the consumption of the mediator. The findings of the 1 min shake-flask experiments are shown in Table 1.

Table 1. Percentages of electron donor consumed during one minute two-phase reactions, percentage of electron donor used for hydrogen peroxide production and total number of transferred electrons per molecular oxygen reduced in two-phase experiments (2 mM DMFc and 100 μM catalyst in DCB).^{II}

System	Electron donor consumed, %	NaI method		TiOx method	
		<i>n</i>	<i>r</i> _{H₂O₂} , %	<i>n</i>	<i>r</i> _{H₂O₂} , %
Co ₂ (DPO) + DMFc	100	3.7	15	3.6	22
Co ₂ (DPOx) + DMFc	100	3.8	12	3.7	13
Co ₂ (DPX) + DMFc	100	3.9	7	3.7	16
CoTPP + DMFc	100	3.6	19	3.8	12
DMFc ^a	66	3.2	37	3.1	44
Co ₂ (DPOx) + DMFc ^b	100	3.8	11	3.8	8
Co ₂ (DPOx) + TTF	100	3.2	41	3.2	42
Co ₂ (DPOx) + TTF ^a	100	3.5	24	3.5	24

^a Reaction time 10 minutes; ^b DCE as a solvent

The presence of the catalyst increased the rate of the reaction by a factor of between 50-100, but both hydrogen peroxide and water were produced.^{II} All the catalysts under consideration showed reasonable selectivity towards four-electron reduction of molecular oxygen after 1 minute of reaction, the best one being Co₂(DPX) (NaI method). Additionally no significant effect due to the use of a different solvent was observed. Overall, the results of Table 1 obtained by two different analytical methods are in reasonable agreement, considering the low amounts of titrated hydrogen peroxide. The comparison of the reactions using TTF (not active for hydrogen peroxide reduction) and DMFc as electron donors show that a significant amount of hydrogen peroxide was observed with TTF,^{II} contradicting previous results.^{103,147} The yield of hydrogen peroxide produced with TTF decreased when the reaction time was increased to 10 min, suggesting that cobalt porphyrins could catalyse the decomposition of hydrogen peroxide. This was confirmed by H₂O₂ decomposition experiments with the cell described in Scheme 5A. During the 2 min reaction hydrogen peroxide concentration decreased by *ca.* 5 %, and most of the hydrogen peroxide was lost after one hour.^{II} Similar results were obtained with only DFcE in the DCE phase.^I If Co₂(DPOx) was used instead of CoTPP, losses of hydrogen peroxide were 11 and 34% after 1 and 10 min reactions, respectively. The hydrogen peroxide reduction was also investigated in an anaerobic glove box with the cell composition described in Scheme 5B. The concentration of hydrogen peroxide decreased by 46% during 1 minute of reaction and no DMFc was detected with the UME voltammetry.^{II}

A		B
5 mM BATB	1 mM H ₂ O ₂	5 mM BATB
2 mM DMFc	10 mM HCl	2 mM DMFc
100 μM Co ₂ (DPX)		100 μM Co ₂ (DPX)
or 1 mM CoTPP		
Oil	Water	Oil

Scheme 5. Schematic representation of the initial composition of the aqueous phase and the organic phase for the biphasic hydrogen peroxide decomposition (A) and reduction (B) experiments.^{II}

Based on these measurements, it seems that the species in the organic phase catalyse the decomposition of hydrogen peroxide to molecular oxygen and water. Biphasic experiments with TTF show that Co₂(DPOx) catalyses hydrogen peroxide decomposition and it seems to also be able to catalyse the reduction of H₂O₂ to water. Thus, selectivity towards water deduced from biphasic experiments is overestimated, especially at longer periods of time.^{II} The differentiation between hydrogen peroxide disproportionation to water and oxygen followed by four-electron oxygen reduction and the direct reduction of hydrogen peroxide by

a two electron process is very difficult. Therefore, a complete understanding of the catalyst selectivity cannot be achieved with these biphasic experiments.

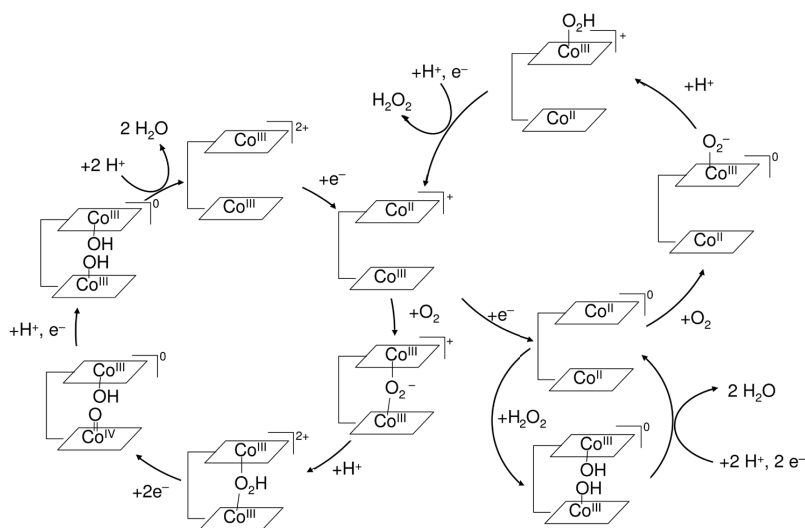
To explain these results, oxygen reduction catalysed by Co₂(DPX) was investigated in more detail by calculating the binding energies of oxygen and various reaction products on the catalyst by DFT.^{II} The binding energies of molecular oxygen inside (“dock-in”) and outside (“dock-on”) the Co₂(DPX) molecule for both neutral and +1 charged catalyst are shown in Table 2. The calculations indicate that a significant amount of oxygen reduction proceeds on the outside of the cofacial porphyrins, not only inside, as previously considered, as the binding energy for the “dock-on” site is considerably higher ($z = 0$) or equal ($z = +1$).

Table 2. Binding energy of O₂ to Co₂(DPX) from the DFT calculations.^{II}

$E_{\text{bind}} / \text{eV}$	$z = 0$	$z = +1$
O ₂ inside Co ₂ (DPX)	0.36	0.44
O ₂ outside Co ₂ (DPX)	0.66	0.44

The computational results confirm that the reduction to hydrogen peroxide takes place when oxygen is bound on the “exo” side (“dock-on”) of the catalyst, while four-electron reduction takes place with oxygen bound on the “endo” side (“dock-in”) of the molecule.^{II} Since the catalyst is initially in a neutral form, oxygen will bind on the Co₂(DPX), leading to hydrogen peroxide production. After desorption of H₂O₂ from the molecule, Co₂(DPX) will have a +1 charge, so both “dock-on” and “dock-in” paths are equally favourable in the terms of binding energy. The first reduction step in the “dock-on” cycle can either take place before or after complex formation with oxygen, because oxygen is also likely to bind on the top of Co₂(DPX)⁺.^{II} Moreover DMFc is also able to reduce Co₂(DPX)⁺ to the neutral form.¹⁴⁷ The “dock-on/dock-in” mechanism is shown in Scheme 6.

Hydrogen peroxide reduction was shown to occur inside the Co₂(DPX) cavity by dissociation of HOOH and formation of a Co^{III}-OH HO-Co^{III} complex (also the intermediate of oxygen reduction inside the catalyst), followed by addition of two protons and two electrons (“dock-in” mechanism for H₂O₂ reduction), confirming the fast hydrogen peroxide reduction observed experimentally.^{II}



Scheme 6. The “dock-on/dock-in” mechanism for oxygen reduction catalysed by cofacial biscobalt porphyrins based on computational and experimental results. The “dock-on” path on the top right shows the production of hydrogen peroxide on the catalyst and the “dock-in” path on the left shows the production of water inside the catalyst. The “dock-in” path on the lower right shows the reduction of hydrogen peroxide inside the catalyst.¹¹

The experiments performed with TTF indicate that the reaction proceeds significantly by the “dock-on” path as predicted by the computational results, producing mostly hydrogen peroxide. H_2O_2 can then be reduced inside the catalyst or decomposed to oxygen and water, as indicated by the decreasing H_2O_2 yield with the increasing reaction time.¹¹ The differences between the earlier results suggesting mostly four-electron reduction and this work can be attributed to the effects of the graphite electrode on the conformation of the adsorbed porphyrins. Adsorbed porphyrins most likely form stacks, so that oxygen coordinated on the porphyrin is also coordinated by another cobalt atom on the “exo” side of another biscobalt porphyrin. Similar behaviour has been observed with cobalt porphine, which forms dimers on an electrode surface.¹⁴⁹ Also, the driving force effect could explain the observed differences: cofacial porphyrins have been shown to catalyse oxygen reduction to hydrogen peroxide at high overpotentials even when the four-electron reduction is taking place at lower overpotentials.¹⁵⁰ The thermodynamic driving force of the reaction in DCB could be high enough to favour the “dock-on” path.

These findings also differ from the result obtained for homogeneous oxygen reduction catalysed by $\text{Co}_2(\text{DPOx})$ in benzonitrile.¹⁴⁷ As there is a 0.36 V difference in the driving force for the oxygen reduction in benzonitrile and in DCB,¹¹ this difference could play a crucial role in the selectivity, so that the reaction proceeds through the “dock-in” path in benzonitrile and

“dock-on” path in DCB or DCE. On the other hand, the explanation may be as simple as the competitive coordination of the counter ions and oxygen to the cobalt atoms. All the earlier results have been obtained with more strongly coordinating anions (for example ClO_4^-) compared to TB^- used in this work¹⁵¹ and it is well known that anions which are non-coordinating in aqueous solution, such as ClO_4^- , NO_3^- , and BF_4^- are found to be coordinating in non-aqueous solutions.^{152,153} Thus it is likely that coordination of perchlorate will compete with the coordination of oxygen on the catalyst, thus inhibiting the “dock-on” path, but weakly coordinating anions like TB^- are not able to bind to metal centres strongly enough to significantly affect the oxygen binding. ClO_4^- also has a higher charge density than TB^- , so it associates more strongly with positively charged species by outer-sphere complexation. In addition, benzonitrile can coordinate to the cobalt atoms, blocking the adsorption sites of oxygen, as it is a more coordinative solvent than DCB. As a result, the counter anion will bind on the positive Co^{III} -atom, thus complicating the electron transfer from the donor. As seen from Scheme 6, this is the critical point: accepting the electron from donor promotes “dock-on” path, but if this site is blocked by tightly bound perchlorate, the “dock-in” path is favoured instead. The displacement of less strongly coordinating TB^- is easier than the displacement of perchlorate and thus the “dock-on” path is also more active. These results indicate that the selectivity of the cofacial porphyrins could be tuned by the choice of ligands or anions present in the solution, as indicated by DFT calculations of stabilization effect of the anions on $\text{H}_4\text{TPP}^{2+}$.¹⁴² The calculations show that counter anion binds to the protonated porphyrin much more strongly than oxygen, and the effect is more significant with smaller anions with binding energies of the complex following the order of: $\text{Cl}^- > \text{PF}_6^- \gg \text{TB}^-$.¹⁴²

To translate these results to biological insights, the structure of cofacial porphyrins can be compared with the structure of cytochrome *c* oxidase. In *CcO*, the central metal of the porphyrin ring is coordinated from below by histidine, so that the protein structure prevents the coordination of oxygen outside the catalyst, blocking the “dock-on” path. The results of this publication show that this protection is important. If the environment around the metal centres remains unprotected, hydrogen peroxide production will take place instead of the desired four-electron reduction and hydrogen peroxide can be very harmful to proteins. Yet inside the catalyst, the hydrogen peroxide is safely dissociated by the metal centres and reduced to water. Thus, the next step in designing a bioinspired oxygen reduction catalyst would be to block the outer face of the porphyrin system.

6 Proton Transfer Catalysed Reactions at Liquid-Liquid Interfaces

Another type of catalysis utilised at liquid-liquid interfaces more familiar for organic chemists is the so called “phase transfer catalysis” (PTC). It is a widespread synthetic method to catalyse reactions between reagents soluble in immiscible phases. In a typical PTC reaction the addition of a “phase transfer catalyst”, typically a tetra-alkyl ammonium cation, facilitates the transfer of reactive anions from an aqueous phase to an organic phase, allowing the reaction to occur.¹⁵⁻¹⁷ The standard textbook explanation is that the quaternary ammonium cations shuttles the reactant anions and the corresponding anions produced in the reaction across the liquid-liquid interface.¹⁵⁻¹⁷ The “electrochemical” interpretation is that the partition of the “phase transfer catalyst” between the phases defines the Galvani potential difference across the interface according to the Nernst-Donnan equation.⁵⁸ This interfacial polarisation is the driving force for other ion transfer reactions that controls the distribution of ions between the phases. The validity of this interpretation has been established by using a potentiostat instead of a partitioning ion to adjust the Galvani potential difference and hence the rate of the reaction.¹⁵⁴⁻¹⁵⁸

Proton transfer catalysis can be considered as an extension of phase transfer catalysis. In this case acid catalysed reactions are performed without addition of organic acids, but instead protons transferred across the ITIES are used to catalyse reactions in the oil phase. In Publication III, we demonstrate an electrochemically driven S_N1 reaction, where a proton transferred into the organic phase either electrochemically or by a “phase transfer catalyst” catalyses a S_N1 substitution on ferrocene methanol (FcMeOH).

6.1 Cyclic Voltammetry of Ferrocene Methanol in a Four-Electrode Cell

The synthesis of FcMeOH was described in 1958.¹⁵⁹ It is highly stable in aqueous solutions exhibiting a reversible one-electron oxidation and has become a common redox probe in electrochemistry, scanning electrochemical microscopy¹⁶⁰⁻¹⁶² and sensors^{163,164}. Since ferrocene derivatives like DcMfc, DMfc, and DFcE^I have been previously proposed as electron donors in oxygen reduction at liquid-liquid interfaces,^{78,137} FcMeOH was also investigated for this purpose. However, the behaviour of FcMeOH was remarkably different from other ferrocene derivatives, although its redox potential is close to that of the ferrocene (−0.02 V vs. Fc/Fc⁺)^{III}. The cyclic voltammograms of 5 mM FcMeOH in DCB is shown in

Figure 18A, and the effect of the FcMeOH concentration on the voltammetry is shown in Figure 18B.

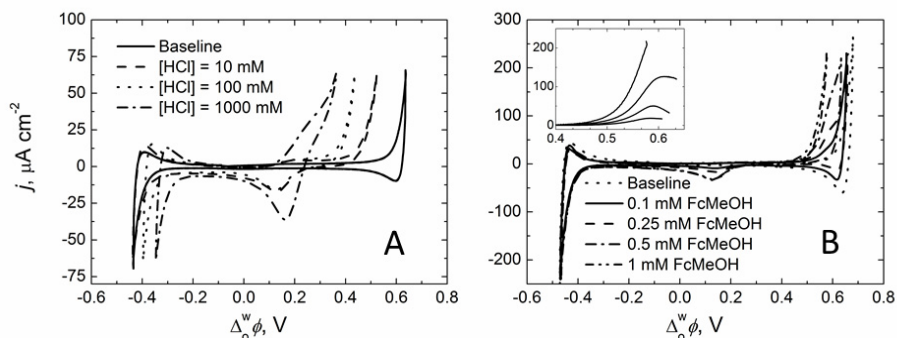


Figure 18. A) pH dependence of the voltammograms of 5 mM FcMeOH in DCB. Baseline: 5 mM BATB in DCB and 10 mM HCl. B) Effect of the FcMeOH concentration on the voltammetry, with the baseline subtracted positive scans shown in the inset (with 1 mM FcMeOH giving the highest current and 0.1 mM FcMeOH the lowest).^{III}

The positive limit of the potential window is determined by proton transfer, shifting in the negative direction with increasing proton concentration as dictated by the Nernst equation. Adding FcMeOH to the organic phase shifts the positive limit of the potential window by more than 100 mV in the negative direction, and the magnitude of the shift increases with increasing proton concentration. This indicates that FcMeOH facilitates proton transfer. The shift of *ca.* 70-90 mV with decreasing pH at the positive limit of the potential window indicates that the process is a one proton transfer per FcMeOH.^{III} The larger observed shift probably arises from differences in iR compensation between each measurement.

Furthermore, no return peak is observed after the reversal of the scan direction, indicating that the protons are consumed in the oil phase. This is similar to the proton-coupled electron transfer wave observed for oxygen reduction by DcMFC, where the latter acts as a proton acceptor to form a hydride species, which in turn reacts with oxygen to form hydrogen peroxide (see Section 4.2).⁷⁸ However, DcMFC is a much stronger reducing agent (0.04 V vs. aqueous SHE⁷⁹) and the proton transfer wave is shifted less with DcMFC than with FcMeOH. If Fc is used instead, the behaviour resembles the base line, indicating that oxygen reduction by Fc is slow.¹³⁷ Very efficient catalysts like cofacial biscobalt porphyrins are needed to observe a similar shift in the onset potential of proton transfer and the sigmoidal shape of the wave.^{II} The ferrocene derivatives without the -OH group are able to slightly facilitate proton transfer from water to the oil phase by protonation of the metal core, and the rate of the

following oxygen reduction reaction increases with decreasing redox potential (DcMfc > DMFc > Fc). Yet with FcMeOH the facilitation effect for H⁺ transfer is very large and the rate of the following chemical reaction very high, comparable to reactions catalysed by efficient oxygen reduction catalysts like cofacial biscobalt porphyrins.^{II} This indicates that the reaction mechanism between FcMeOH and H⁺ is very different from other ferrocene derivatives, and can be described as facilitated proton transfer followed by chemical reaction.

When the experiment was done under a nitrogen atmosphere, the results were similar to those obtained in the presence of oxygen, confirming that molecular oxygen does not participate in the reaction.^{III} Figure 18 also shows reversible chloride transfer at the negative limit of the potential window (wave potential shifts ca. 50-60 mV per log [Cl⁻]), and an ion transfer wave at ca. 0.16 V assigned to FcMeOH⁺. It is worth noticing that this wave is irreversible, indicating that FcMeOH⁺ reacts further in the aqueous acidic solution. Figure 18B shows that the decrease in the FcMeOH concentration shifts the proton transfer wave to more positive potentials, and at [FcMeOH] = 0.1 mM the voltammogram becomes almost identical with the base line. This confirms that FcMeOH is able to facilitate proton transfer. At FcMeOH concentrations of 0.25 mM and 0.5 mM a diffusion limited peak for proton transfer is clearly visible, although it overlaps with the unassisted proton transfer wave. At 1 mM the transfer is independent of the FcMeOH concentration at the used conditions, as no peak is observed (a peak would be observed if the scan would be done at a slower scan rate to higher potentials). The base line subtracted voltammogram measured for 0.25 mM FcMeOH shows a clear irreversible peak with a half-wave potential of 0.57 V. The Nernst equation for this facilitated proton transfer process can be described as shown in Equation 23⁷

$$\Delta_{\circ}^w \phi_{1/2} = \Delta_{\circ}^w \phi_{H^+}^{o'} + \frac{RT}{2F} \ln \left(\frac{D_L}{D_{LH^+}} \right) - \frac{RT}{F} \ln K_{LH^+} c_{H^+,w} \quad (23)$$

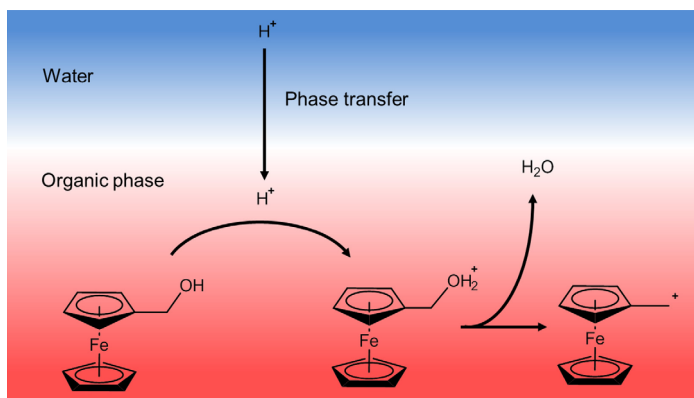
where $\Delta_{\circ}^w \phi_{1/2}$ and $\Delta_{\circ}^w \phi_{H^+}^{o'}$ are the observed half-wave potential of LH⁺ and formal transfer potential of H⁺ (0.677 V at the w-DCB interface), respectively. LH⁺ stands for the protonated complex, D represents the diffusion coefficient of species in the oil phase, K_{LH^+} is the equilibrium constant of the protonation reaction of L and $c_{H^+,w}$ is the aqueous proton concentration. If the effect of the protonation on the diffusion coefficient of FcMeOH is assumed to be negligible, the association constant calculated from Equation 23 is 6450 M⁻¹.^{III} The calculated value is actually only the apparent association constant, as the complexation

may not reach equilibrium because of the following chemical reaction. However, the half-wave potential of the facilitated proton transfer does not shift significantly with increasing FcMeOH concentration, indicating that the effect of the chemical reaction step on the observed facilitated transfer is small.

Since FcMeOH is soluble in both aqueous and organic solvents, the partition coefficient of FcMeOH between DCB and 10 mM HCl solution was determined to be 82 based on the decrease of the absorption intensity of FcMeOH in the DCB phase at the wavelength of 448 nm.^{III} Hence the equilibrium concentration of FcMeOH in the aqueous phase is 61 μM for 5 mM of FcMeOH in DCB phase. FcMeOH can also be protonated in the aqueous phase and transferred into the oil phase, but the expected peak current density would be *ca.* 10 $\mu\text{A cm}^{-2}$ (at the scan rate of 50 mV s^{-1}). As the measured currents for facilitated proton transfer on the positive end of the potential window in Figure 18A are much higher, the facilitated proton transfer wave is mostly due to FcMeOH in the oil phase. The exact mechanism of the facilitated transfer is difficult to determine, but the possibilities include the partition of FcMeOH into the aqueous phase followed by aqueous complexation and transfer, transfer by interfacial complexation, transfer followed by organic-phase complexation, or a combination of these.^V

6.2 Proton Transfer Catalysed $\text{S}_{\text{N}}1$ Substitution to Ferrocene Methanol

In Publication III ferrocene methanol protonation in the presence of oxygen was studied by ultramicroelectrode redox voltammetry and electrospray ionization mass spectrometry (ESI-MS). ESI-MS results show that the irreversible chemical reaction following the facilitated proton transfer by FcMeOH observed by four-electrode cell voltammetry can in fact be attributed to elimination of the hydroxyl group and formation of a remarkably stable α -ferrocenyl carbocation, as shown by online ESI-MS measurements.^{III} The reaction scheme for proton transfer catalysed α -ferrocenyl carbocation formation is described in Scheme 7.



Scheme 7. “Proton transfer catalysed” interfacial formation of α -ferrocenyl carbocations from FcMeOH.^{III}

Formation of the stable α -ferrocenyl carbocations¹⁶⁵⁻¹⁶⁸ is actually well-known since the 1960s, as described in the review by Neuse.¹⁶⁹ Ferrocene compounds were used to catalyze combustion processes in the booster rockets designed for both civil and military aerospace applications, but the low sublimation temperature of ferrocene reduced the long-term stability of the propellants. To overcome this problem, numerous research projects aiming to develop simple and cheap synthesis methodologies for ferrocenyl polymers were launched. It was discovered that the linear poly-(ferrocenylene-methylene) with the mass range of *ca.* 1000-2000 units could be readily prepared in FcMeOH melt in an acid catalysed self-polymerization reaction under nitrogen atmosphere. This polymerization was enabled by the formation of the stable α -ferrocenyl carbocation.^{168,169}

The ESI-MS results for the samples taken from a shake-flask reaction between 5 mM FcMeOH in DCB and 5 mM LiTB and 10 mM HCl in aqueous phase under aerobic conditions at given reaction times are shown in Figure 19 and the relative abundances of the species as a function of reaction time are shown in Figure 20.^{III}

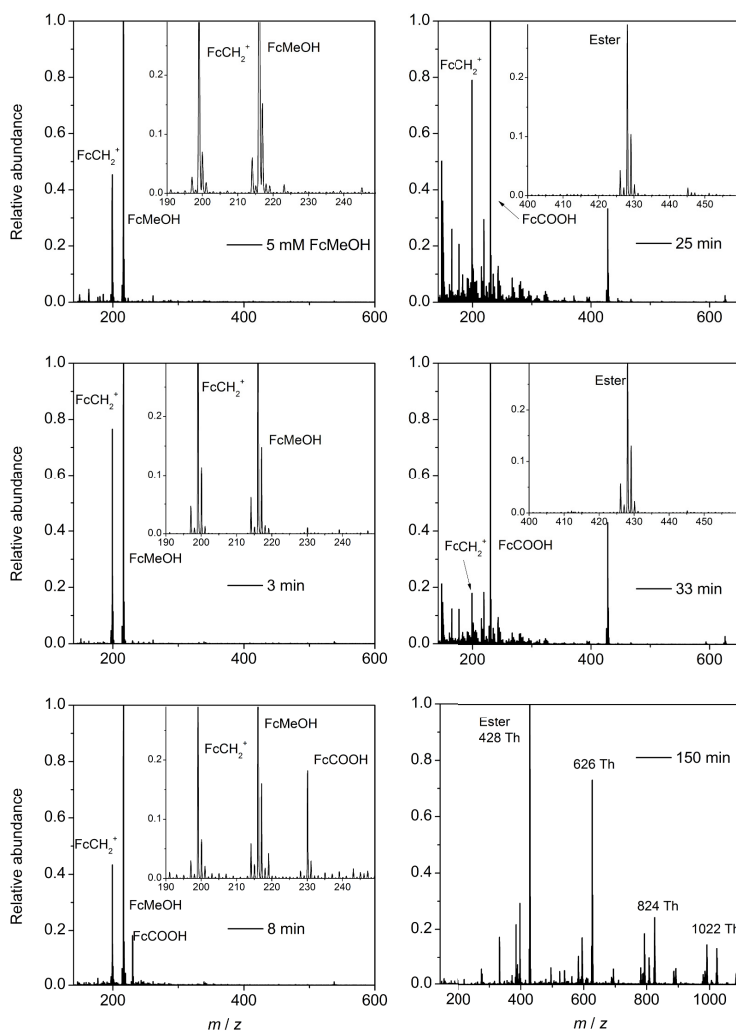


Figure 19. The ESI-MS results of samples extracted from the reaction system (equal amounts of 5 mM FcMeOH in DCB and 5 mM LiTB + 10 mM HCl in aqueous phase) at different reaction times. The insets show the observed isotope distribution of the peaks.^{III}

The distinctive isotope distribution of iron (54, 6.3%; 56, 100%; 57, 2.4%; 58, 0.3%) was used to identify the iron-containing species. In the mass spectrum of FcMeOH significant peaks around 216 Th (m/z) were observed corresponding well to the calculated isotope distribution of FcMeOH (214, 6.3%; 215, 0.8%; 216, 100%; 217, 14.5%; 218, 1.4%), indicating the generation of FcMeOH⁺ ions (the oxidation of Fe(II) to Fe(III)) during ESI. Also significant peaks showing the distinctive isotope distribution of iron were observed around 199 Th, indicating a reaction product from FcMeOH. The shift of m/z (-17 Da) corresponds to the elimination of the hydroxyl group and formation of a carbocation (FcCH₂⁺, m/z = 199).^{III} This carbocation is stabilized by the high electron donating property of the

ferrocenyl group.^{165,167} Additional peaks around 230 Th were observed in the sample taken from the oil phase of a batch reaction after 8 minutes of reaction showing the typical isotope distribution of iron (Figure 19). These peaks were assigned to ferrocene carboxylic acid FcCOOH, indicating that the carbocations can further react with molecular oxygen to produce FcCOOH and H⁺ (See Scheme 8). The produced acid could then react with FcMeOH, forming the corresponding ester (*m/z* = 428) observed after 25 min of batch reaction, but a more likely option is the reaction with the carbocation, as almost no FcMeOH was left when the formation of the ester began (Figure 20).^{III} The reaction proceeded slowly after the ester formation by the additions of 198 mass units giving products with *m/z* = 626, 824 and 1022. This corresponds to the addition of the carbocation (and loss of one proton), probably by substitution of a proton in 1,2-, 1,3- and 1,1'-ringpositions, as in the case of ferrocenyl alcohol polymerization from melts under nitrogen.¹⁶⁹

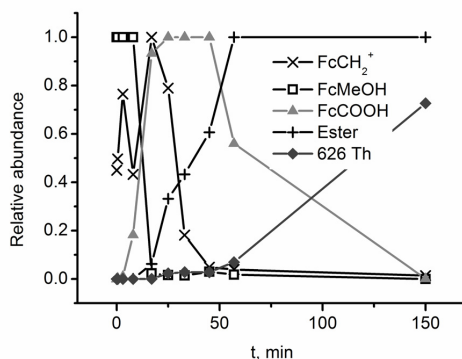


Figure 20. The relative abundance of the species as a function of time.^{III}

The products of the shake flask reactions in the oil phase were also characterized by ultramicroelectrode measurements. After 10 minutes of reaction adsorption obviously blocked the surface of the carbon fibre microelectrode, and no sigmoidal waves were observed. In contrast, on a Pt UME, a wave assigned for FcMeOH was observed (Figure 21), followed by a smaller wave on a positive scan. A desorption peak followed by the FcMeOH redox wave was observed on the return scan. This behaviour is probably due to the adsorption of the carbocation on the electrode surface. Also the response of the Pt UME is lost after longer reaction times, due to contamination of the surface as could be seen with an optical microscope.^{III}

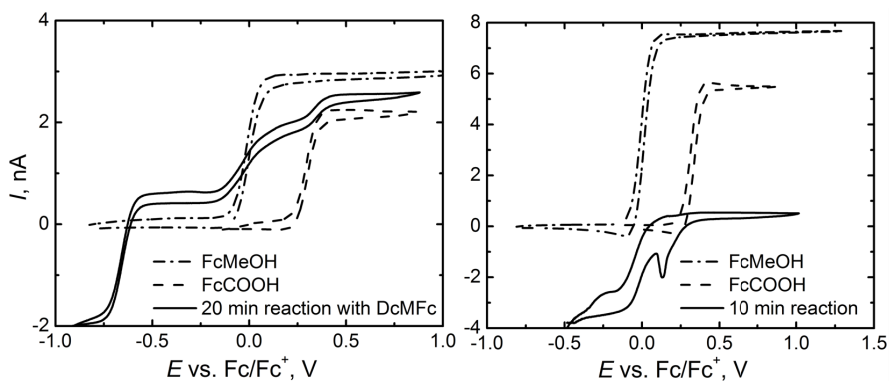
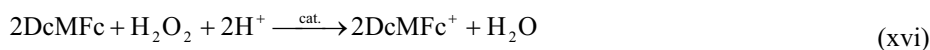
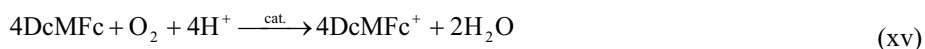
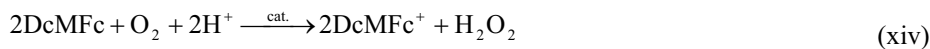


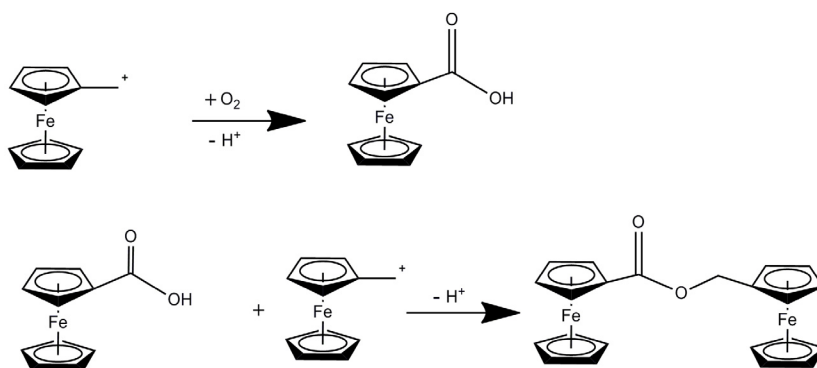
Figure 21. UME voltammograms of 2.5 mM FcMeOH and FcCOOH with 10 μm carbon fibre UME (Left) and with 25 μm Pt UME (Right). Left: voltammogram of the sample taken from the oil phase after 20 min reaction and quenched with DcMfc (10 μm carbon fibre UME). Right: UME voltammogram of the sample taken from the oil phase after 10 min reaction (25 μm Pt UME), not quenched.^{III}

However, if the reaction in the sample was quenched with equal amount of 5 mM DcMfc, clear sigmoidal waves could be observed, as shown in Figure 21. The addition of DcMfc has two effects on the system: i) DcMfc reduces most of the oxidized ferrocene derivatives, as it is strong reducing agent. ii) protons extracted in the oil phase are quickly consumed by oxygen and hydrogen peroxide reduction, catalysed by the platinum wire, according to the Reactions xiv-xvi.^{III}



Two clear oxidation waves in Figure 21 correspond well with the wave measured for pure FcMeOH and with the wave for FcCOOH at *ca.* 0.30 V *vs.* Fc/Fc⁺, in agreement with the ESI-MS observations. The redox wave observed at -0.67 V *vs.* Fc/Fc⁺ corresponds to reduction/oxidation of DcMfc. The diffusion coefficients of $6.1 \times 10^{-6} \text{ cm}^2 \text{ s}^{-1}$ for FcMeOH and $4.4 \times 10^{-6} \text{ cm}^2 \text{ s}^{-1}$ for FcCOOH were determined from the limiting currents.^{III} Curiously, a sample taken after 20 min of reaction gave an almost identical response as one taken after 30 min of reaction. After 45 min the signal had disappeared almost completely even for the quenched samples. The formation of the carbocation can be considered as an equilibrium reaction. Addition of DcMfc consumes protons and increases the amount of water in the system, driving the equilibrium towards FcMeOH. According to Figure 20, the formation of ester begins after 20 minutes of reaction, so the amount of observed FcCOOH and FcMeOH

should decrease. However, this is not observed in UME measurements. Plausible explanations could be hydrolysis of the ester to FcCOOH and FcMeOH after quenching the solution with DcMFC, or that the formation of ester does not have a significant effect on the redox potentials of the ferrocenyl groups. The proposed reaction sequence following the protonation of FcMeOH in the presence of oxygen is described in Scheme 8.



Scheme 8. Reactions of α -ferrocenyl carbocation in the shake flask experiments in the presence of oxygen.^{III}

More interestingly, in a presence of equimolar amount of indole the proton transfer catalysed $\text{S}_{\text{N}}1$ substitution of indole on FcMeOH was clearly observed by ESI-MS. The reaction (Figure 22)¹⁷⁰⁻¹⁷² was performed in a batch reaction and the results were analysed by ESI-MS.^{III} After 5 min batch reaction between 5 mM FcMeOH and indole in DCB and 5 mM LiTB and 10 mM HCl in water the MS spectra showed the presence of a small amount of FcCOOH and 3-(ferrocenylmethyl)-1H-indole (315 Th). After 20 min of reaction the 3-(ferrocenylmethyl)-1H-indole peaks were dominant, as shown in Figure 22.

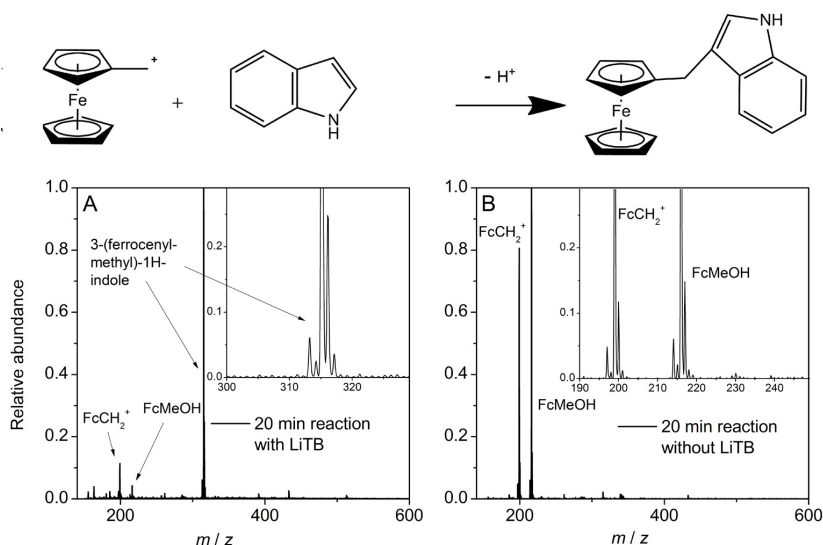


Figure 22. Top: The reaction between α -ferrocenyl carbocation and indole, producing 3-(ferrocenylmethyl)-1H-indole.¹⁷⁰⁻¹⁷² Below: The ESI-MS results of oil phase samples from the shake flask experiments with 5 mM FcMeOH and indole in DCB and 10 mM HCl with (A) and without (B) 5 mM LiTB in water after 20 min of reaction. The inset shows the isotope distribution of the peaks.^{III}

The control experiment with only 10 mM HCl in the aqueous phase was performed to show that the polarisation of the interface by the presence of a “phase-transfer catalyst” is critical to allow the reaction, as now no reaction was observed after 20 min.^{III} In summary, we have shown that proton transfer across the organic-water interface provides an excellent method for controlled “proton transfer catalysed” ferrocenyl carbocation formation, which can be utilised in S_N1 substitution to ferrocenyl alcohols. The proton flux across the interface can be adjusted by adjusting the Galvani potential difference across the interface, either by a potentiostat or by an appropriate choice of salts. A controllable method for carbocation formation could be very beneficial for synthesis of a wide range of metallocene derivatives, as ferrocene derivatives have shown anti-anemic and cytotoxic properties, and some show significant anticancer activity.¹⁷³ Furthermore, these compounds are widely used in bio-organometallic chemistry.¹⁷⁴ The synthesis taking place at liquid-liquid interfaces could also be used to control stereoselectivity of the reactions by introduction of suitable surface active groups to the reactant molecules. Biphasic ESI-MS was shown to be an efficient tool to understand and characterise biphasic reactions.

7 Fuel Cell Utilising a Liquid-Liquid Interface

Nowadays, most hydrogen peroxide is produced by the organic auto-oxidation process, primarily the anthraquinone process. For the process to be economically viable, large scale plants are needed. Unfortunately the storage, handling and transportation of hydrogen peroxide is inherently hazardous due to its strongly oxidizing nature.¹⁷⁵ The risks can be reduced by addition of stabilizers to prevent hydrogen peroxide decomposition, but this limits the usage of H_2O_2 for medicinal purposes.¹⁷⁵ For these reasons, an economic method for small scale on-site production of hydrogen peroxide would be beneficial, and hence hybrid fuel cells capable of producing both power and H_2O_2 have been investigated as an alternative.¹⁷⁶⁻¹⁷⁸

In Publication IV a novel type of a flow fuel cell utilising a liquid-liquid interface, with the oil phase gelled with PVC, was demonstrated for hydrogen peroxide production (see Figure 23).

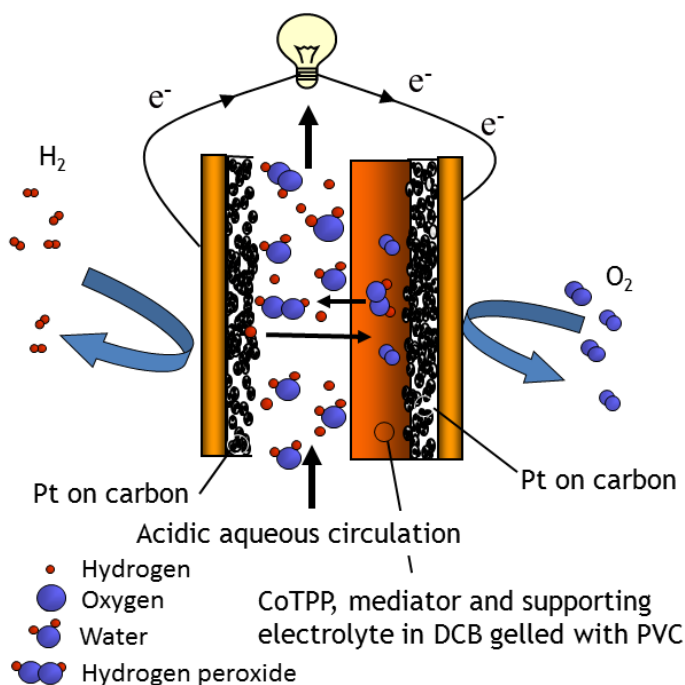


Figure 23. The concept of the flow fuel cell.^{IV}

The operating principle of this kind of fuel cell is to have the hydrogen oxidation reaction in the anode as in a normal fuel cell, but the oxygen reduction reaction takes place at the liquid-liquid interface as described in Sections 4.2 and 5.2, and not at the cathode. The oxidized

mediator produced at the interface would then be reduced at the cathode. The electrons from hydrogen oxidation are taken through an external circuit to be consumed in the electrode reaction at the cathode. The cell reactions are shown below:^{IV}



In theory, the cell should have the same open circuit voltage as a normal fuel cell for H_2O_2 production,^{IV} but the observed value would differ due to some mixed potential effects. Hydrogen peroxide produced at the interface would be extracted into the aqueous phase, and could be recovered from the aqueous circulation. The cyclic voltammetry measurements in Figure 24 show that the system is controlled by the liquid-liquid interface, with a similar response as from a four-electrode cell. Both the catalyst and the mediator are needed to produce the PCET peak, as was observed in four-electrode cell measurements.^{IV}

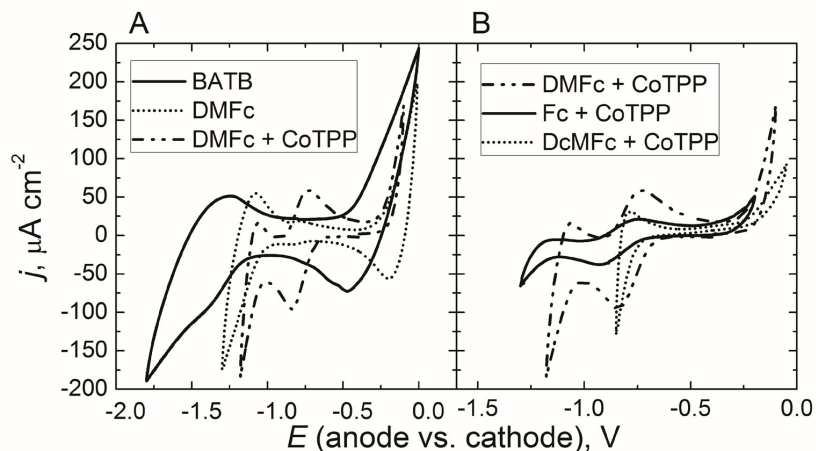


Figure 24. CVs of 5 mM BATB (black), 5 mM BATB + DMFc (red) and 5 mM BATB + DMFc + 1 mM CoTPP (blue) in gelled DCB phase measured with the flow fuel cell (left), and the effect of the different mediators on the potential window (right). Scan rate: 50 mV s^{-1} .^{IV}

For positive current to flow through the cell, hydrogen oxidation takes place at the anode, transfer of ions occurs at the ITIES (transfer of H^+ or M^+ from aqueous to oil phase or transfer of Cl^- from oil phase aqueous phase) and the mediator is regenerated at the cathode. In the case of negative currents, hydrogen evolution takes place at the anode, transfer of mediator from oil to water or transfer of chloride from water to oil occurs at the ITIES and mediator is

oxidised at the cathode. The cell reactions in the presence of both mediator and catalyst at the positive end of the potential window are shown in Figure 25A and at the negative end in Figure 25B.^{IV}

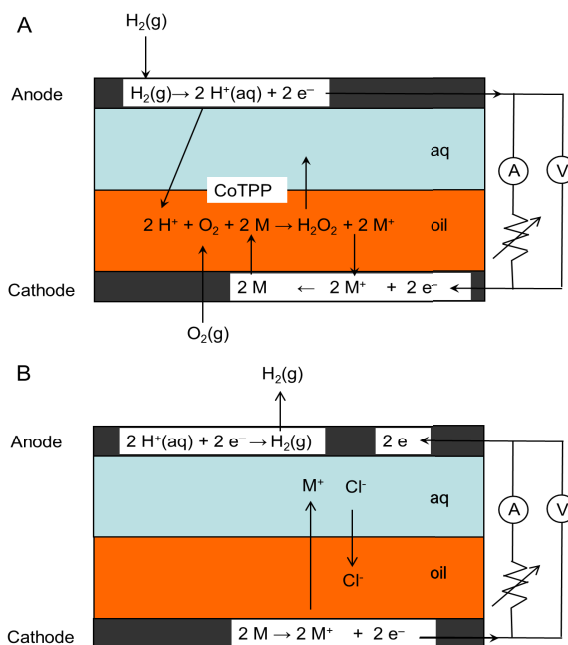


Figure 25. Cell reactions for positive (A) and negative (B) currents in Figure 24B.^{IV}

The cell was operated as an electrolyser in long term constant current experiments, with the anode potential higher than the cathode potential, as the performance of the fuel cell was not good enough to sustain the reasonable current densities. Hydrogen peroxide production of 3.8 mg/l with an efficiency of 58% ($25 \mu\text{A cm}^{-2}$, 1 h) was demonstrated, but the efficiency decreased at longer time scale.^{IV} This was probably due to the reduction and decomposition of H_2O_2 .^{I,II} Current densities achieved with the cell are rather modest, due to the small interfacial area compared to the interfacial area obtained with the porous carbon electrode normally utilised in a fuel cell. Additionally, the current density was limited by the diffusion of the mediator. However, this work confirms that electrocatalysis at liquid-liquid interfaces can be utilised in a fuel cell or an electrolyser.

8 Conclusions

This thesis investigates the applications of proton transfer across the liquid-liquid interface for oxygen reduction and synthesis of organic chemicals. Proton transfer can be controlled by applying a suitably high Galvani potential difference across the interface either chemically or with an external power source, and oxygen reduction is initiated by the transfer of protons into the oil phase in the presence of an electron donor. When 1,2-diferrocenyloethane was used as a donor, it was shown to facilitate proton transfer across the interface by forming DFcEH⁺. Oxygen was then slowly reduced in the oil phase due to the low thermodynamic driving force. Initially it was suspected that only one DFcE molecule would be needed to reduce oxygen to hydrogen peroxide, but the results showed that the reaction proceeded by oxidation of a ferrocene unit to form DFcE⁺ until all the DFcE had reacted. This was then followed by slower oxidation of the other ferrocenyl unit to give DFcE²⁺. Methylation of the ferrocenyl rings would decrease the redox potential of the compound, and this kind of a redox mediator could prove to be very interesting for hydrogen evolution. More interestingly, the results showed that DFcE is able to reduce hydrogen peroxide, and the reaction is actually faster than oxygen reduction. DFcE was also shown to catalyse decomposition of hydrogen peroxide. This confirms that great care has to be taken when using ferrocene derivatives as electron donors for oxygen reduction, since distinguishing four-electron reduction of molecular oxygen from two-electron reduction followed by H₂O₂ reduction and decomposition is very difficult.

The rate of oxygen reduction can be increased by addition of a catalyst. Cofacial biscobalt porphyrins, synthetic analogues for the active centre of cytochrome *c* oxidase, were found to be efficient catalysts for oxygen reduction at liquid-liquid interfaces. The reaction was found to produce mainly water and some hydrogen peroxide, but the mediator had a significant effect on the selectivity. Mostly water was produced when 1,1'-dimethylferrocene was used as the redox mediator, but significant amounts of hydrogen peroxide were produced if tetrathiafulvalene was used instead, contradicting the previous results in the literature. Density functional theory calculations indicated that cofacial porphyrins actually catalyse oxygen reduction to hydrogen peroxide when oxygen is bound on the “exo” side (“dock-on”) of the catalyst, while four-electron reduction takes place with oxygen bound on the “endo” side (“dock-in”) of the molecule, favouring the “dock-on” path. As a result a new “dock-on/dock-in” mechanism was proposed. These results are important because they give insight into the mechanistic operation of the active centres in enzymes. In the case of CcO the “dock-on” sites

are blocked, leading to “dock-in” path and four-electron reduction of molecular oxygen to water. The results also provide important insight for the design of improved oxygen reduction catalysts, which is important, as one of the main barriers for the replacement of the current hydrocarbon economy is the need for cheap and efficient ways to reduce oxygen to replace expensive platinum.

Furthermore, this thesis demonstrates that proton transfer across the liquid-liquid interface could also be used to catalyse the synthesis of organic chemicals. In the case of ferrocenyl alcohols, generation of α -ferrocenyl carbocations by protonation of the OH group and consequent elimination of water was initiated by the transfer of protons into the organic phase, providing a new method for synthesis of ferrocene derivatives. The proton flux and hence the reaction rate could be controlled by the addition of a suitable phase-transfer catalyst anion or by external polarisation with a potentiostat. If ferrocene methanol was dissolved in the oil phase in the presence of oxygen, proton transfer across the interface catalysed the production of ferrocene carboxylic acid. The reaction then proceeded by producing the corresponding ester and finally a multiferrocenyl polymer. In the presence of a suitable nucleophile, for example indole, the reaction gave 3-(ferrocenylmethyl)-1H-indole as the product. This is a completely new kind of an approach to perform acid catalysed organic reactions. Additionally, the utility of the biphasic electrospray ionization mass spectrometry to characterize reaction products of complex reactions was demonstrated.

Finally, a concept of a fuel cell utilising a liquid-liquid interface was presented. Hydrogen was oxidized on the anode as in a normal fuel cell, but oxygen reduction was catalysed by a molecular catalyst, cobalt porphyrin, at the liquid-liquid interface instead of the cathode. The redox mediator oxidised at the interface was regenerated on the cathode, completing the electric circuit. This novel paradigm shows that heterogeneous molecular catalysts could be utilised in a fuel cell for the production of hydrogen peroxide. The system was controlled by the charge transfer across the liquid-liquid interface, limiting the system performance. Current densities and amounts of hydrogen peroxide produced with the fuel cell were rather poor, but there are number of ways to improve the performance, as described in Section 8.1.

In summary, this thesis presents how proton transfer across the liquid-liquid interface can be utilised to better understand the mechanism of oxygen reduction by ferrocene derivatives and the electrocatalysis of oxygen reduction by molecular catalysts. The results are relevant for fundamental understanding and the development of biomimetic catalysts for oxygen

reduction. Also, the concept of proton transfer catalysed chemical reactions is introduced, where acid catalysed reactions can be controlled by using the external polarisation to control the proton transfer rate. This thesis demonstrates that proton transfer across an ITIES is a useful means to drive oxygen reduction or acid catalysed reactions in the oil phase, both for understanding the reaction mechanisms and for practical applications.

8.1 Recommendations for Further Work

It would be interesting to continue to work with multiferrocenyl compounds, both for oxygen reduction and hydrogen evolution. By careful choice of the substituents the redox potentials of these compounds could be lowered to the range where uncatalysed oxygen reduction would be reasonably fast, and hydrogen evolution would be thermodynamically favourable. This kind of work could give better understanding of the reaction mechanisms.

Cofacial porphyrins are shown to be effective biomimetic oxygen reduction catalysts. To improve the selectivity for four-electron reduction of molecular oxygen, the “dock-on” sites should be blocked, either by some suitable ligands or by steric hindrance of these sites. Additionally, porphyrins with electron donors substituted on the porphyrin ring could prove to be very interesting catalysts for oxygen reduction.

To improve the fuel cell performance, the liquid-liquid interface could be polarised with a common ion. Hence ion transfer across the interface would not limit the system any more, and better performance would be expected. To increase the surface area of the liquid-liquid interface, microemulsions could be utilised. To decrease the effects of the H_2O_2 decomposition, the use of transition metal containing components should be avoided. One way would be to use free-base porphyrins with tetrathiafulvalene as the redox mediator.

Publication III is the first paper utilising proton transfer catalysed reactions for synthesis of organic compounds. This work could be built on by performing other acid catalysed reactions without the addition of organic acids. Also interactions of the reactants with the interface could be utilised to exert some control over the stereochemistry of the products.

References

1. C. Gavach, *Experientia*, **18** (1971) 321-331.
2. C. Gavach, A. Savajols, *Electrochim. Acta*, **19** (1974) 575-581.
3. C. Gavach, P. Seta, F. Henry, *Bioelectrochem. Bioenerg.*, **1** (1974) 329-342.
4. C. Gavach, F. Henry, *J. Electroanal. Chem.*, **54** (1974) 361-370.
5. Z. Samec, V. Mareček, J. Koryta, M.W. Khalil, *J. Electroanal. Chem.*, **83** (1977) 393-397.
6. J. Koryta, *Electrochim. Acta*, **24** (1979) 293-300.
7. D. Homolka, L.Q. Hung, A. Hofmanova, M.W. Khalil, J. Koryta, V. Marecek, Z. Samec, S.K. Sen, P. Vanysek, *Anal. Chem.*, **52** (1980) 1606-1610.
8. J. Koryta, M. Březina, A. Hofmanová, D. Homolka, L.Q. Hung, W. Khalil, V. Mareček, Z. Samec, S.K. Sen, P. Vanýsek, J. Weber, J. Heyrovský, *Bioelectrochem. Bioenerg.*, **7** (1980) 61-68.
9. J. Koryta, *Ion-Sel. Electrode Rev.*, **5** (1983) 61-68.
10. M.A. Méndez, R. Partovi-Nia, I. Hatay, B. Su, P. Ge, A. Olaya, N. Younan, M. Hojeij, H.H. Girault, *Phys. Chem. Chem. Phys.*, **12** (2010) 15163-15171.
11. N.S. Lewis, D.G. Nocera, *Proc. Natl. Acad. Sci.*, **103** (2006) 15729-15735.
12. P.E.M. Siegbahn, M.R.A. Blomberg, *Chem. Rev.*, **110** (2010) 7040-7061.
13. E. Kim, E.E. Chufán, K. Kamaraj, K.D. Karlin, *Chem. Rev.*, **104** (2004) 1077-1134.
14. M.Z. Cremer, *J. Biol.*, **47** (1906) 562-608.
15. M. Mieczyslaw, *Pure Appl. Chem.*, **72** (2000) 1399-1403.
16. D. Albanese, *Catal. Rev.: Sci. Eng.*, **45** (2003) 369-395.
17. M. Mąkosza, M. Fedoryński, *Catal. Rev.: Sci. Eng.*, **45** (2003) 321-367.
18. W. Nernst, E.H. Riesenfeld, *Ann. der Physik*, **313** (1902) 600-608.
19. J.T. Davies, S.E. Rideal, *Can. J. Chem.*, **33** (1955) 947-960.
20. Z. Samec, V. Mareček, J. Weber, *J. Electroanal. Chem.*, **96** (1979) 245-247.
21. Z. Samec, V. Mareček, J. Weber, *J. Electroanal. Chem.*, **103** (1979) 11-18.
22. T. Kakutani, T. Osakai, M. Senda, *Bull. Chem. Soc. Jpn.*, **4** (1983) 991-996.
23. D. Homolka, V. Mareček, *J. Electroanal. Chem.*, **112** (1980) 91-96.
24. Z. Samec, D. Homolka, V. Mareček, *J. Electroanal. Chem.*, **135** (1982) 265-283.
25. B. Hundhammer, T. Solomon, H. Alemu, *J. Electroanal. Chem.*, **149** (1983) 179-183.
26. Z. Samec, V. Mareček, D. Homolka, *J. Electroanal. Chem.*, **126** (1981) 121-129.
27. H.H. Girault, D.J. Schiffrin, in: A.J. Bard (Ed) *Electroanalytical chemistry*, Marcel Dekker, New York, 1989, pp. 1-142.

28. R.A. Iglesias, S.A. Dassie, *Ion Transfer at Liquid/Liquid Interfaces*, Nova Publishers, New York, 2010.
29. L.J. Sanchez Vallejo, J.M. Ovejero, R.A. Fernández, S.A. Dassie, *Int. J. Electrochem.*, **2012** (2012) 34.
30. R.A.W. Dryfe, in: S.A. Rice (Ed) *Advances in Chemical Physics*, John Wiley & Sons, Inc., Hoboken, NJ, 2009, pp. 153-215.
31. Z. Samec, *Electrochim. Acta*, **84** (2012) 21-28.
32. Y. Shao, J.A. Campbell, H.H. Girault, *J. Electroanal. Chem.*, **300** (1991) 415-429.
33. T. Kakiuchi, J. Noguchi, M. Senda, *J. Electroanal. Chem.*, **336** (1992) 137-152.
34. E.J.W. Verwey, K.F. Niessen, *Philos. Mag.*, **28** (1939) 435-446.
35. C. Gavach, P. Seta, B. D'Epenoux, *J. Electroanal. Chem.*, **83** (1977) 225-235.
36. H.H. Girault, D.J. Schiffrin, *J. Electroanal. Chem.*, **150** (1983) 43-49.
37. W. Schmickler, in: A. Volkov, G. (Ed) *Liquid Interfaces in Chemical, Biological and Pharmaceutical Applications*, Marcel Dekker, New York, 2001, pp. 183-212.
38. W. Schmickler, *J. Electroanal. Chem.*, **426** (1997) 5-9.
39. R.D. Webster, D. Beaglehole, *Phys. Chem. Chem. Phys.*, **2** (2000) 5660-5666.
40. I. Benjamin, *J. Chem. Phys.*, **96** (1992) 577-585.
41. I. Benjamin, *J. Chem. Phys.*, **97** (1992) 1432-1445.
42. D. Michael, I. Benjamin, *J. Phys. Chem.*, **99** (1995) 1530-1536.
43. J. Strutwolf, A.L. Barker, M. Gonsalves, D.J. Caruana, P.R. Unwin, D.E. Williams, J.R.P. Webster, *J. Electroanal. Chem.*, **483** (2000) 163-173.
44. G. Luo, S. Malkova, J. Yoon, D.G. Schultz, B. Lin, M. Meron, I. Benjamin, P. Vanýsek, M.L. Schlossman, *J. Electroanal. Chem.*, **593** (2006) 142-158.
45. G. Luo, S. Malkova, J. Yoon, D.G. Schultz, B. Lin, M. Meron, I. Benjamin, P. Vanýsek, M.L. Schlossman, *Science*, **311** (2006) 216-218.
46. N. Laanait, J. Yoon, B. Hou, P. Vanysek, M. Meron, B. Lin, G. Luo, I. Benjamin, M.L. Schlossman, *J. Chem. Phys.*, **132** (2010) 171101.
47. A. Volkov, G., D.W. Deamer, *Liquid-Liquid Interfaces: Theory and Methods*, CRC Press, Boca Raton, FL, 1996.
48. A.G. Volkov, D.W. Deamer, D.L. Tanelian, V.S. Markin, *Prog. Surf. Sci.*, **53** (1996) 1-134.
49. I. Benjamin, *Science*, **261** (1993) 1558-1560.
50. K.J. Schweighofer, I. Benjamin, *J. Electroanal. Chem.*, **391** (1995) 1-10.
51. K.J. Schweighofer, I. Benjamin, *J. Phys. Chem.*, **99** (1995) 9974-9985.
52. H.H. Girault, *J. Electroanal. Chem.*, **257** (1988) 47-55.

53. A.J. Parker, *Electrochim. Acta*, **21** (1976) 671-679.
54. R. Schurhammer, G. Wipff, *J. Mol. Struct.*, **500** (2000) 139-155.
55. S. Wilke, T. Zerihun, *J. Electroanal. Chem.*, **515** (2001) 52-60.
56. B. Hundhammer, C. Müller, T. Solomon, H. Alemu, H. Hassen, *J. Electroanal. Chem.*, **319** (1991) 125-135.
57. A.J. Olaya, P. Ge, H.H. Girault, *Electrochem. Commun.*, **19** (2012) 101-104.
58. T. Kakiuchi, in: A. Volkov, G., D.W. Deamer (Eds), *Liquid-liquid interfaces, Theory and Methods*, CRC Press, Boca Raton, 1996, pp. 1-18.
59. A.J. Bard, L.R. Faulkner, *Electrochemical methods : fundamentals and applications*, 2nd ed., John Wiley & Sons, New York, 2001.
60. P. Walden, *Z. Phys. Chem.*, **55** (1906) 207-249.
61. P.W. Atkins, *Physical Chemistry*, 4th ed., Oxford University Press, Oxford, 1990.
62. T. Osakai, K. Ebina, in: A. Volkov, G. (Ed) *Liquid Interfaces in Chemical, Biological and Pharmaceutical Applications*, Marcel Dekker, New York, 2001, pp. 27-62.
63. Y. Shao, A.A. Stewart, H.H. Girault, *J. Chem. Soc., Faraday Trans.*, **87** (1991) 2593-2597.
64. F.O. Laforge, P. Sun, M.V. Mirkin, *J. Am. Chem. Soc.*, **128** (2006) 15019-15025.
65. P. Sun, F.O. Laforge, M.V. Mirkin, *J. Am. Chem. Soc.*, **129** (2007) 12410-12411.
66. V.J. Cunnane, L. Murtomäki, in: A. Volkov, G., D.W. Deamer (Eds), *Liquid/Liquid Interfaces: Theory and Methods*, CRC Press, Boca Raton, 1996, pp. 401-416.
67. H.H. Girault, *Analytical and Physical Electrochemistry*, EPFL Press, Lausanne, 2004.
68. I. Hatay, B. Su, F. Li, M.A. Méndez, T. Khoury, C.P. Gros, J.M. Barbe, M. Ersoz, Z. Samec, H.H. Girault, *J. Am. Chem. Soc.*, **131** (2009) 13453-13459.
69. A. Sabela, V. Mareček, Z. Samec, R. Fuoco, *Electrochim. Acta*, **37** (1992) 231-235.
70. P. Luehring, A. Schumpe, *J. Chem. Eng. Data*, **34** (1989) 250-252.
71. N.A. Kotov, M.G. Kuzmin, *J. Electroanal. Chem.*, **285** (1990) 223-240.
72. N. Eugster, H. Jensen, D.J. Fermín, H.H. Girault, *J. Electroanal. Chem.*, **560** (2003) 143-149.
73. Z. Samec, N. Eugster, D.J. Fermín, H.H. Girault, *J. Electroanal. Chem.*, **577** (2005) 323-337.
74. D. Schaming, M. Hojeij, N. Younan, H. Nagatani, H.J. Lee, H.H. Girault, *Phys. Chem. Chem. Phys.*, **13** (2011) 17704-17711.
75. N. Nishi, S. Imakura, T. Kakiuchi, *Anal. Chem.*, **78** (2006) 2726-2731.
76. R.O. Rahn, M.I. Stefan, J.R. Bolton, E. Goren, P.-S. Shaw, K.R. Lykke, *Photochem. Photobiol.*, **78** (2003) 146-152.

77. R.M. Sellers, *Analyst*, **105** (1980) 950-954.
78. B. Su, R. Partovi-Nia, F. Li, M. Hojeij, M. Prudent, C. Corminboeuf, Z. Samec, H.H. Girault, *Angew. Chem., Int. Ed.*, **47** (2008) 4675-4678.
79. J.J. Nieminen, I. Hatay, P. Ge, M.A. Méndez, L. Murtomäki, H.H. Girault, *Chem. Commun.*, **47** (2011) 5548-5550.
80. F. Gao, Y. Yang, J. Liu, H. Shao, *Ionics*, **16** (2010) 45-50.
81. M. Prudent, Eacute, M.A. Ndez, H.H. Girault, *Anal. Sci.*, **24** (2008) 1399-1404.
82. M. Prudent, M.A. Mendez, D.F. Jana, C. Corminboeuf, H.H. Girault, *Metallomics*, **2** (2010) 400-406.
83. M.A. Méndez, M. Prudent, B. Su, H.H. Girault, *Anal. Chem.*, **80** (2008) 9499-9507.
84. T.J. Stockmann, Y. Lu, J. Zhang, H.H. Girault, Z. Ding, *Chem.–Eur. J.*, **17** (2011) 13206-13216.
85. M.A. Méndez, Z. Nazemi, I. Uyanik, Y. Lu, H.H. Girault, *Langmuir*, **27** (2011) 13918-13924.
86. R.A. Hartvig, M.A. Méndez, M.v.d. Weert, L. Jorgensen, J. Østergaard, H.H. Girault, H. Jensen, *Anal. Chem.*, **82** (2010) 7699-7705.
87. A.O. Allen, C.J. Hochanadel, J.A. Ghormley, T.W. Davis, *J. Phys. Chem.*, **56** (1952) 575-586.
88. J.T. Mueller, P.M. Urban, *J. Power Sources*, **75** (1998) 139-143.
89. D.R. Weinberg, C.J. Gagliardi, J.F. Hull, C.F. Murphy, C.A. Kent, B.C. Westlake, A. Paul, D.H. Ess, D.G. McCafferty, T.J. Meyer, *Chem. Rev.*, **112** (2012) 4016-4093.
90. S. Hammes-Schiffer, *Acc. Chem. Res.*, **42** (2009) 1881-1889.
91. M.H.V. Huynh, T.J. Meyer, *Chem. Rev.*, **107** (2007) 5004-5064.
92. K. Kinoshita, *Electrochemical Oxygen Technology*, John Wiley & Sons, New York, 1992.
93. V.J. Cunnane, G. Geblewicz, D.J. Schiffrin, *Electrochim. Acta*, **40** (1995) 3005-3014.
94. H. Ohde, K. Maeda, Y. Yoshida, S. Kihara, *J. Electroanal. Chem.*, **483** (2000) 108-116.
95. P. Liljeroth, B.M. Quinn, K. Kontturi, *Langmuir*, **19** (2003) 5121-5127.
96. F. Li, B. Su, F.C. Salazar, R.P. Nia, H.H. Girault, *Electrochem. Commun.*, **11** (2009) 473-476.
97. A.J. Olaya, P. Ge, J.F. Gonthier, P. Pechy, C. Corminboeuf, H.H. Girault, *J. Am. Chem. Soc.*, **133** (2011) 12115-12123.
98. A. Trojáněk, J. Langmaier, Z. Samec, *Electrochim. Acta*, **82** (2012) 457-462.

99. I. Hatay, B. Su, F. Li, R. Partovi-Nia, H. Vrubel, X. Hu, M. Ersoz, H.H. Girault, *Angew. Chem., Int. Ed.*, **48** (2009) 5139-5142.
100. B. Su, I. Hatay, P.Y. Ge, M. Mendez, C. Corminboeuf, Z. Samec, M. Ersoz, H.H. Girault, *Chem. Commun.*, **46** (2010) 2918-2919.
101. T.E. Bitterwolf, A.C. Ling, *J. Organomet. Chem.*, **40** (1972) C29-C32.
102. V. Fomin, *Russ. J. Gen. Chem.*, **77** (2007) 954-960.
103. C.J. Chang, Z.H. Loh, C. Shi, F.C. Anson, D.G. Nocera, *J. Am. Chem. Soc.*, **126** (2004) 10013-10020.
104. J.P. Collman, P. Denisevich, Y. Konai, M. Marrocco, C. Koval, F.C. Anson, *J. Am. Chem. Soc.*, **102** (1980) 6027-6036.
105. N. Eugster, D.J. Fermín, H.H. Girault, *J. Phys. Chem. B*, **106** (2002) 3428-3433.
106. D.J. Fermín, H.D. Duong, Z. Ding, P.F. Brevet, H.H. Girault, *Phys. Chem. Chem. Phys.*, **1** (1999) 1461-1467.
107. T.E. Bitterwolf, A.C. Ling, *J. Organomet. Chem.*, **57** (1973) C15-C18.
108. J. Lubach, W. Drenth, *Recl. Trav. Chim. Pays-Bas*, **92** (1973) 586-592.
109. D.J. Schiffrin, Y. Cheng, International Seminar on Charge Transfer at Liquid/Liquid and Liquid/Membrane Interfaces, Kyoto, 1996.
110. R. Lahtinen, C. Johans, S. Hakkarainen, D. Coleman, K. Kontturi, *Electrochem. Commun.*, **4** (2002) 479-482.
111. C. Johans, P. Liljeroth, K. Kontturi, *Phys. Chem. Chem. Phys.*, **4** (2002) 1067-1071.
112. A. Trojánek, J. Langmaier, Z. Samec, *Electrochem. Commun.*, **8** (2006) 475-481.
113. R. M. Lahtinen, D. J. Fermín, H. Jensen, K. Kontturi, H. H. Girault, *Electrochem. Commun.*, **2** (2000) 230-234.
114. I. Hatay, P.Y. Ge, H. Vrubel, X. Hu, H.H. Girault, *Energy Environ. Sci.*, **4** (2011) 4246-4251.
115. B. Hinnemann, P.G. Moses, J. Bonde, K.P. Jørgensen, J.H. Nielsen, S. Horch, I. Chorkendorff, J.K. Nørskov, *J. Am. Chem. Soc.*, **127** (2005) 5308-5309.
116. P. Ge, M.D. Scanlon, P. Peljo, X. Bian, H. Vubrel, A. O'Neill, J.N. Coleman, M. Cantoni, X. Hu, K. Kontturi, B. Liu, H.H. Girault, *Chem. Commun.*, **48** (2012) 6484-6486.
117. Y. Li, H. Wang, L. Xie, Y. Liang, G. Hong, H. Dai, *J. Am. Chem. Soc.*, **133** (2011) 7296-7299.
118. X. Bian, J. Zhu, L. Liao, M.D. Scanlon, P. Ge, C. Ji, H.H. Girault, B. Liu, *Electrochem. Commun.*, **22** (2012) 128-132.

119. L.I. Boguslavsky, A.A. Kondrashin, I.A. Kozlov, S.T. Metelsky, V.P. Skulachev, A.G. Volkov, *FEBS Lett.*, **50** (1975) 223-226.
120. A.G. Volkov, *Anal. Sci.*, **14** (1998) 19-25.
121. A.G. Volkov, *Electrochim. Acta*, **44** (1998) 139-153.
122. B. Su, H.H. Girault, Z. Samec, in: E. Santos, W. Schmickler (Eds), *Catalysis in Electrochemistry*, John Wiley & Sons, Inc., Hoboken, NJ, 2011, pp. 427-451.
123. M.I. Gugeshashvili, A.G. Volkov, L.S. Yaguzhinsky, A.F. Mironov, L.I. Boguslavsky, *Bioelectrochem. Bioenerg.*, **10** (1983) 493-498.
124. D.G. Georganopoulou, D.J. Caruana, J. Strutwolf, D.E. Williams, *Faraday Discuss.*, **116** (2000) 109-118.
125. T. Sugihara, H. Hotta, T. Osakai, *Phys. Chem. Chem. Phys.*, **6** (2004) 3563-3568.
126. B. Su, I. Hatay, F. Li, R. Partovi-Nia, M.A. Méndez, Z. Samec, M. Ersoz, H.H. Girault, *J. Electroanal. Chem.*, **639** (2010) 102-108.
127. I. Hatay Patir, *J. Electroanal. Chem.*, **685** (2012) 28-32.
128. R. Jasinski, *Nature*, **201** (1964) 1212-1213.
129. Y. Li, S. Wu, B. Su, *Chem.–Eur. J.*, **18** (2012) 7372-7376.
130. I. Hatay Patir, *Electrochim. Acta*, **87** (2013) 788-793.
131. P. Peljo, *Biomimetic Oxygen Reduction at Liquid-Liquid Interfaces: From Electrocatalysis to Fuel Cell Applications*, Licentiate's thesis, Aalto University, Espoo, 2012.
132. A. Trojánek, V. Mareček, H. Jänchenová, Z. Samec, *Electrochem. Commun.*, **9** (2007) 2185-2190.
133. R. Partovi-Nia, B. Su, F. Li, C.P. Gros, J.M. Barbe, Z. Samec, H.H. Girault, *Chem.–Eur. J.*, **15** (2009) 2335-2340.
134. S. Fukuzumi, S. Mochizuki, T. Tanaka, *Inorg. Chem.*, **28** (1989) 2459-2465.
135. S. Fukuzumi, S. Mochizuki, T. Tanaka, *Chem. Lett.*, **18** (1989) 27-30.
136. R. Partovi-Nia, B. Su, M.A. Méndez, B. Habermeyer, C.P. Gros, J.M. Barbe, Z. Samec, H.H. Girault, *ChemPhysChem*, **11** (2010) 2979-2984.
137. B. Su, I. Hatay, A. Trojánek, Z. Samec, T. Khoury, C.P. Gros, J.M. Barbe, A. Daina, P.A. Carrupt, H.H. Girault, *J. Am. Chem. Soc.*, **132** (2010) 2655-2662.
138. I. Hatay, B. Su, M.A. Méndez, C. Corminboeuf, T. Khoury, C.P. Gros, M. Bourdillon, M. Meyer, J.M. Barbe, M. Ersoz, S. Záliš, Z. Samec, H.H. Girault, *J. Am. Chem. Soc.*, **132** (2010) 13733-13741.
139. S. Wu, B. Su, *Chem.–Eur. J.*, **18** (2012) 3169-3173.

140. A. Trojánek, J. Langmaier, B. Su, H.H. Girault, Z. Samec, *Electrochem. Commun.*, **11** (2009) 1940-1943.
141. A. Trojaneek, J. Langmaier, S. Zalis, Z. Samec, *Chem. Commun.*, **48** (2012) 4094-4096.
142. A. Trojaneek, J. Langmaier, J. Sebera, S. Zalis, J.-M. Barbe, H.H. Girault, Z. Samec, *Chem. Commun.*, **47** (2011) 5446-5448.
143. A.J. Olaya, D. Schaming, P.-F. Brevet, H. Nagatani, T. Zimmermann, J. Vanicek, H.-J. Xu, C.P. Gros, J.-M. Barbe, H.H. Girault, *J. Am. Chem. Soc.*, **134** (2012) 498-506.
144. R. Boulatov, J.P. Collman, I.M. Shiryayeva, C.J. Sunderland, *J. Am. Chem. Soc.*, **124** (2002) 11923-11935.
145. Z. Halime, H. Kotani, Y. Li, S. Fukuzumi, K.D. Karlin, *Proc. Natl. Acad. Sci.*, **108** (2011) 13990-13994.
146. C.J. Chang, Y. Deng, C. Shi, C.K. Chang, F.C. Anson, D.G. Nocera, *Chem. Commun.*, (2000) 1355-1356.
147. S. Fukuzumi, K. Okamoto, C.P. Gros, R. Guillard, *J. Am. Chem. Soc.*, **126** (2004) 10441-10449.
148. J. Rosenthal, D.G. Nocera, *Acc. Chem. Res.*, **40** (2007) 543-553.
149. E. Song, C. Shi, F.C. Anson, *Langmuir*, **14** (1998) 4315-4321.
150. J.P. Collman, N.H. Hendricks, C.R. Leidner, E. Ngameni, M. L'Her, *Inorg. Chem.*, **27** (1988) 387-393.
151. W.E. Geiger, F. Barrière, *Acc. Chem. Res.*, **43** (2010) 1030-1039.
152. M.R. Rosenthal, *J. Chem. Educ.*, **50** (1973) 331.
153. S.H. Strauss, *Chem. Rev.*, **93** (1993) 927-942.
154. C. Forssten, K. Kontturi, L. Murtomäki, H.C. Hailes, D.E. Williams, *Electrochem. Commun.*, **3** (2001) 379-383.
155. V.J. Cunnane, D.J. Schiffrin, C. Beltran, G. Geblewicz, T. Solomon, *J. Electroanal. Chem.*, **247** (1988) 203-214.
156. S.N. Tan, R.A. Dryfe, H.H. Girault, *Helv. Chim. Acta*, **77** (1994) 231-242.
157. Y.-T. Kong, S.-i. Imabayashi, T. Kakiuchi, *J. Am. Chem. Soc.*, **122** (2000) 8215-8219.
158. Y.-T. Kong, T. Kakiuchi, *J. Electroanal. Chem.*, **446** (1998) 19-23.
159. G.D. Broadhead, J.M. Osgerby, P.L. Pauson, *J. Chem. Soc.*, (1958) 650-656.
160. P. Liljeroth, C. Johans, C.J. Slevin, B.M. Quinn, K. Kontturi, *Electrochem. Commun.*, **4** (2002) 67-71.
161. B.M. Quinn, I. Prieto, S.K. Haram, A.J. Bard, *J. Phys. Chem. B*, **105** (2001) 7474-7476.

162. D. Momotenko, F. Cortes-Salazar, A. Lesch, G. Wittstock, H.H. Girault, *Anal. Chem.*, **83** (2011) 5275-5282.
163. P. Audebert, C. Demaille, C. Sanchez, *Chem. Mater.*, **5** (1993) 911-913.
164. C. Bourdillon, C. Demaille, J. Moiroux, J.-M. Saveant, *J. Am. Chem. Soc.*, **116** (1994) 10328-10329.
165. J.H. Richards, E.A. Hill, *J. Am. Chem. Soc.*, **81** (1959) 3484-3485.
166. D.S. Trifan, R. Bacskai, *Tetrahedron Lett.*, **1** (1960) 1-8.
167. E.A. Hill, J.H. Richards, *J. Am. Chem. Soc.*, **83** (1961) 3840-3846.
168. E.W. Neuse, D.S. Trifan, *J. Am. Chem. Soc.*, **85** (1963) 1952-1958.
169. E. Neuse, *J. Inorg. Organomet. Polym. Mater.*, **15** (2005) 3-31.
170. R. Jiang, C.-X. Yuan, X.-P. Xu, S.-J. Ji, *Appl. Organomet. Chem.*, **26** (2012) 62-66.
171. P.G. Cozzi, L. Zoli, *Green Chem.*, **9** (2007) 1292-1295.
172. P.G. Cozzi, L. Zoli, *Angew. Chem., Int. Ed.*, **47** (2008) 4162-4166.
173. G. Gasser, I. Ott, N. Metzler-Nolte, *J. Med. Chem.*, **54** (2010) 3-25.
174. D.R. van Staveren, N. Metzler-Nolte, *Chem. Rev.*, **104** (2004) 5931-5986.
175. G. Goor, J. Glenneberg, S. Jacobi, *Ullmann's Encyclopedia of Industrial Chemistry*, Wiley-VCH Verlag GmbH & Co. KGaA, 2000.
176. I. Yamanaka, T. Hashimoto, R. Ichihashi, K. Otsuka, *Electrochim. Acta*, **53** (2008) 4824-4832.
177. E. Lobytseva, T. Kallio, N. Alexeyeva, K. Tammeveski, K. Kontturi, *Electrochim. Acta*, **52** (2007) 7262-7269.
178. I. Yamanaka, T. Onizawa, S. Takenaka, K. Otsuka, *Angew. Chem., Int. Ed.*, **42** (2003) 3653-3655.

Electrochemistry at liquid-liquid interfaces is a versatile field of contemporary electrochemistry with applications ranging from electroanalytics to metal extraction.

Many important reactions like photosynthesis or cell respiration (*i.e.* oxygen reduction) take place at the interface between the cell membrane and the surrounding aqueous media, and hence it is natural to study these reactions also at the liquid-liquid interfaces. Oxygen reduction at liquid-liquid interfaces requires transfer of protons into the oil phase in a presence of electron donors. As the proton distribution between the two phases can be adjusted by electrochemical methods, the whole reaction can be controlled very carefully.

This thesis describes how proton transfer at the liquid-liquid interfaces can be used to study catalysed and non-catalysed oxygen reduction and how to utilise these concepts in a development of a novel type of a fuel cell. Additionally, proton transfer controlled synthesis of organic chemicals is also demonstrated.



ISBN 978-952-60-5050-8
ISBN 978-952-60-5049-2 (pdf)
ISSN-L 1799-4934
ISSN 1799-4934
ISSN 1799-4942 (pdf)

Aalto University
School of Chemical Technology
Department of Chemistry
www.aalto.fi

**BUSINESS +
ECONOMY**

**ART +
DESIGN +
ARCHITECTURE**

**SCIENCE +
TECHNOLOGY**

CROSSOVER

**DOCTORAL
DISSERTATIONS**